

Kinematics of Red Variables in the Solar Neighborhood I . Basic Data Obtained by an SiO Maser Survey

Shuji DEGUCHI^{1,2}, Tsuyoshi SAKAMOTO³,
 and

Takashi HASEGAWA⁴

¹*Nobeyama Radio Observatory, National Astronomical Observatory,
 Minamimaki, Minamisaku, Nagano 384-1305*

²*Graduate University for Advanced Studies, National Astronomical Observatory,
 Minamimaki, Minamisaku, Nagano 384-1305*

³*Bisei Space Guard Center, 1716-3 Ookura, Bisei, Ibara, Okayama 714-1411*

⁴*Gunma Astronomical Observatory, 6860-86 Nakayama, Takayama, Agatsuma, Gunma 377-0702*

(Received 2011 April 11; accepted 2011 August 9)

Abstract

In order to study the streaming motions of miras in the Solar neighborhood, we newly surveyed 379 red variables in the SiO maser lines at 42.821 and 43.122 GHz with the Nobeyama 45m radio telescope. Accurate radial velocities were obtained for 229 (220 new) detected stars. The sample is selected from optical variables found by new automated surveys: the Northern Sky Variability Survey and the All Sky Automated Survey. The new sample consists of the "bluer" objects compared with those observed in the previous SiO surveys. The distances to the objects are estimated using the period-luminosity relation, and they are mostly less than 3 kpc from the Sun. The longitude-velocity diagram reveals three prominent groups of stars deviant from the circular Galactic rotation with a flat rotation curve. In addition to the Hercules group of stars which was studied before, we found two new deviant groups: one toward the Perseus arm and the other toward the Sagittarius arm. These two groups both exhibit anomalous motions toward the Galactic center, which seem to be consistent with the noncircular motions of these spiral arms found in the recent VLBI proper-motion measurements for maser gas clumps.

Key words: Galaxy: disk, Galaxy: kinematics and dynamics, stars: AGB and post-AGB

1. Introduction

Moving groups are clumps of stars sharing the same spatial motion in the Solar neighborhood. They are often considered to be a fossil, which keeps past dynamical information after its birth in the Galaxy. The coherent spatial motions of the moving groups are well studied in the past based on the Hipparcos and the RAVE (the Radial Velocity Experiment; Zwitter et al. 2008) databases (see Famaey et al. 2005). In particular, the Hercules group of stars, which was first identified by O. J. Eggen (see a summary by Eggen 1996), is a well studied moving group with rotational lag and outward motion of about 40 km s⁻¹ and 50 km s⁻¹, respectively, to the Galactic rotation. It is inferred that a few percent of stars in the Solar neighborhood are members of this group (Bensby et al. 2007). The origin of the Hercules group is attributed to a rotational resonance of the bar-like Bulge, because the population of stars of this group is a mixture with different ages (Bensby et al. 2007). Feast & Whitelock (2000) investigated an outward motion of short-period Mira variables near the Sun, and attributed it to the resonance effect of the Bulge bar. Presumably the Hercules moving group, which was found in the Solar neighborhood, spreads spatially far from the Sun. Deguchi et al. (2010) found that a group of maser stars in the Galactic longitude range be-

tween 20° and 40°, which are located at a few kpc from the Sun, have a distinctively large outward motion compared with the motions of usual stars under the Galactic rotation. They also attributed the large outward motion to the effect at the outer Lindblad and corotation resonances of the central bar. The resonance effect of the Galactic bar should appear in areas near the resonance circles in the Galactic plane. In particular, the old stars with ages several times longer than the rotational period of the bar pattern reflect the resonance effect. Therefore, miras are ideal sample for studying the bulge-bar resonance effect because they are evolved stars with ages of about a few Gyr. In contrast, tidal streams of dwarf galaxies, e.g., the Sgr dwarf stream (for example, Majewski et al. 2003), are often traced in a relatively limited area of the sky far from the Galactic plane because of their low stellar density, though they still have been found in the Galactic disk using blue metal-poor stars (e.g., Belokurov et al. 2007).

Radial velocities of OH and SiO maser sources have been used to investigate dynamics of stars in the disk (Jiang et al. 1996; Nakashima & Deguchi 2003; Ita et al. 2001) and the bulge of the Galaxy (Izumiura et al. 1995; Sevenster et al. 2001). These maser stars are mostly miras and semi-regular variables, i.e., O-rich evolved stars at the asymptotic-giant-branch (AGB) phase, though a

small amount of red supergiants are contaminated in the sample. Previous surveys of these stars by OH and SiO maser lines were preferentially made for the highly reddened, optically very faint stars because of their high detection rate in a color-selected sample (for example, see Deguchi et al. 2004). These stars are located at relatively large distances in the Galactic disk, compared with a sample of optical miras. Therefore, optical miras in the Solar neighborhood are missing in the previous samples of maser sources [e.g., Nakashima & Deguchi (2003); Deguchi et al. (2007), except Jewell et al. (1991)]. Even though radial velocities have been obtained for a large number of optical miras by optical spectroscopy, the accuracy in the measurement is quite limited. For example, if we compare the radial velocity of a mira in the RAVE database with that of OH or SiO masers, we often find typically a 10 km s^{-1} or much larger difference between them. This is caused by several reasons: insufficient spectral resolution in optical instruments, phase dependency of optical line velocities on mira pulsation (see, e.g., Scholz & Wood 2000), and a velocity shift of the optical lines due to scattering by moving circumstellar dust (van Blerkom & Mao 1982). It is known that the stellar velocities obtained in the maser line measurements are accurate within $\sim 2 \text{ km s}^{-1}$ [e.g., see section 3.1 of Nakashima & Deguchi 2006]. Therefore, it is useful to measure the radial velocities of optical miras in the Solar neighborhood in SiO maser lines even if optical velocities are available for some stars. Moreover, the accurate radial velocities of miras in the Solar neighborhood by the maser observations are essential to see if the deviant stream is continuously connected with the stream that is found previously in a large extension of the Galaxy (Feast & Whitelock 2000; Deguchi et al. 2010). In addition, since precise measurements of proper motions will be available by the phase-reference VLBI technique for SiO maser sources (Kobayashi et al. 2008), accurate 3d motions in space will reveal in future for these objects.

In this paper, we present the result of a new survey of the optical red variables in the SiO maser lines with the 45m telescope at Nobeyama. A number of new variable stars were recently found by automated optical variability surveys: the Northern Sky Variability Survey (NSVS; Woźniak et al. 2004) and the All Sky Automated Survey (ASAS; Pojmanski et al. 2005). Though these newly found optical variables are much bluer in near-infrared (NIR) colors (such as $H - K$) than the typical SiO maser sources previously surveyed, they exhibit the characteristic optical variability of miras. Since the bluer color indicates the higher surface temperature and smaller mass loss rate of the central star in general, the detection rate of SiO masers was expect to be very low for such a sample. However, contrary to our expectation, our preliminary survey made in 2009 resulted in a significantly high detection rate of SiO masers. Therefore, we have performed a new extensive observation in the SiO maser lines toward these red variables, and have increased the data of our SiO radial velocity database. In this paper, we present the result of the observations and give a limited discussion on the kinematic properties of this sample, based mainly on

the radial velocities. For all of the sampled stars, proper motions have been measured optically (Roeser et al. 2010). A kinematic study based on the proper motions will be given in the future paper.

2. Observation, sample selection, and results

2.1. Observation

The observations were made with the 45m radio telescope at Nobeyama in 2009 March, 2010 March–May, and 2010 December–2011 January in the SiO $J=1-0$ $v=1$ and 2 transitions at 43.122 and 42.821 GHz, respectively. A few data taken before 2009 were also added for the present analysis. A cooled HEMT receiver (H40) was used for the 43 GHz observations with acousto-opt spectrometer arrays with 40 and 250 MHz bandwidths (with velocity resolutions of about 0.3 and 1.8 km s^{-1} , respectively). The system temperature was about 180 — 250 K for the SiO observations, depending on weather conditions. The half-power beam width (HPBW) of the telescope was about $40''$ at 43 GHz. A conversion factor of the antenna temperature to the flux density was about 2.9 Jy K^{-1} . All of the observations were made by the position-switching mode. Further details of observations using the NRO 45-m telescope have been described elsewhere (see Deguchi et al. 2000). The spectrometer arrays also covered the SiO $J = 1-0$ $v = 0$ and $v = 3$ lines at 43.424 GHz and 42.519 GHz, respectively, the ^{29}SiO $J = 1-0$ $v = 0$ line at 42.880 GHz, and H53 α at 42.952 GHz. However, these lines were detected in a few sources (shown in Appendix 1).

2.2. Sample selection

The sample for the present SiO maser searches was chosen mainly from the "Catalog of Red Variables in the Northern Sky Variability Survey" (Williams et al. 2004). Because the coverage of this survey is heavily weighted on the northern Galactic plane, we used an additional optical catalog of red variables selected from the "ASAS Variable Stars in Southern Hemisphere" (Pojmanski et al. 2005). These two catalogs listed up the red variables found in automated sky surveys. They give period of optical light curve, classification code, optical magnitude and amplitude, coordinates of the stars with accuracy better than $10''$, and 2MASS and IRAS identifications. From these catalogs, we selected the objects with a classification code of "M" (mira) or "SR+L" (semiregular¹ and irregular variables) and with a period longer than 80 d [which covers enough for SiO maser stars at the short-period limit (~ 150 d)]. Additionally, we applied the selection criteria to effectively squeeze out the stars enshrouded by circumstellar dust; $K < 9$, and $H - K > 0.6$, the $12 \mu\text{m}$ flux density brighter than 3 Jy, and the color $-0.5 < C_{12} [\equiv \log(F_{25}/F_{12})] \lesssim 0.2$, where H and K are 2MASS H and K_s magnitudes, respectively (Cutri et al. 2003), and F_{12} and F_{25} are the IRAS flux densities in the 12 and 25

¹ The variability type, "semi-regular", is applied to the variables with smaller amplitude, shorter periods, and more irregular pulsations than miras; some occasionally show multiple periodicity (Bedding & Zijlstra 1998).

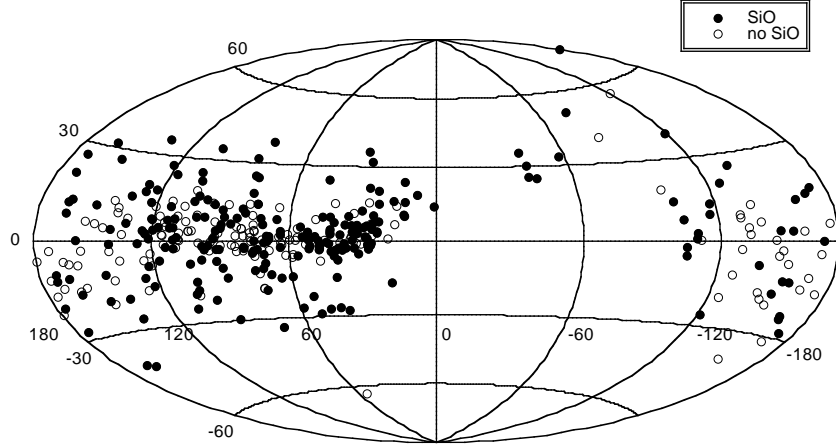


Fig. 1. Distribution of the observed objects in the Galactic coordinates in the Hammer-Aitoff projection. Filled and unfilled circles indicate SiO detection and no detection, respectively.

μm bands, respectively (Beichman et al. 1989) [the MSX bands C and E (Egan et al. 2003) were also consulted for the $|b| \lesssim 6^\circ$ sources. We applied the same criterion in C_{12} by translating $\log(F_E/F_C)$ to C_{12} without any correction, where F_C and F_E are MSX 12 and 21 μm flux densities. Detailed comparison of the MSX colors with those of IRAS (Sjouwerma et al. 2009) showed that the correction is negligibly small around $C_{12} = -0.4$ (see their Figure 4)]. All the objects in the present sample are optically identified variable stars. These are supposedly late-type (AGB or post-AGB) stars surrounded by a dust envelope with a color-temperature range between 250 and 1200 K (they are the stars with a thin dust envelope in region II and IIIa of the mid-IR two-color diagram of van der Veen & Habing 1988). The stars cataloged as a carbon star in the SIMBAD database are excluded from the sample. Furthermore, we selected a few bright objects for backup observations in a bad weather condition. They are slightly bluer sources in $H - K$ and in C_{12} but have not been surveyed before. We added these additional objects to our results for completeness. We have observed all the red variables in the Williams et al. (2004)'s catalog down to $F_{12} = 7$ Jy (though we could not consume all the bright objects in the ASAS catalog). The distribution of the observed stars in the sky is shown in Figure 1.

2.3. Results

Observational results are summarized in Tables 1 and 2 for the SiO detections and no detections, respectively. The observed spectra of the SiO $J = 1 - 0$ $v = 1$ and 2 transitions for detected sources are given in Appendix 1, and the individually interesting objects are also discussed there. Table 3 summarizes a few detections in the additional lines of SiO, i.e., the ^{28}SiO $v = 3$ and $v = 0$ $J = 1 - 0$ and ^{29}SiO $v = 0$ $J = 1 - 0$ transitions [the spectra are shown in Appendix 1]. Table 4 summarizes the infrared properties of all the observed sources.

Figure 2 shows the near- and middle-infrared color-magnitude diagrams for observed stars. If we compare this, for example, with Figure 2 of Deguchi et al. (2010),

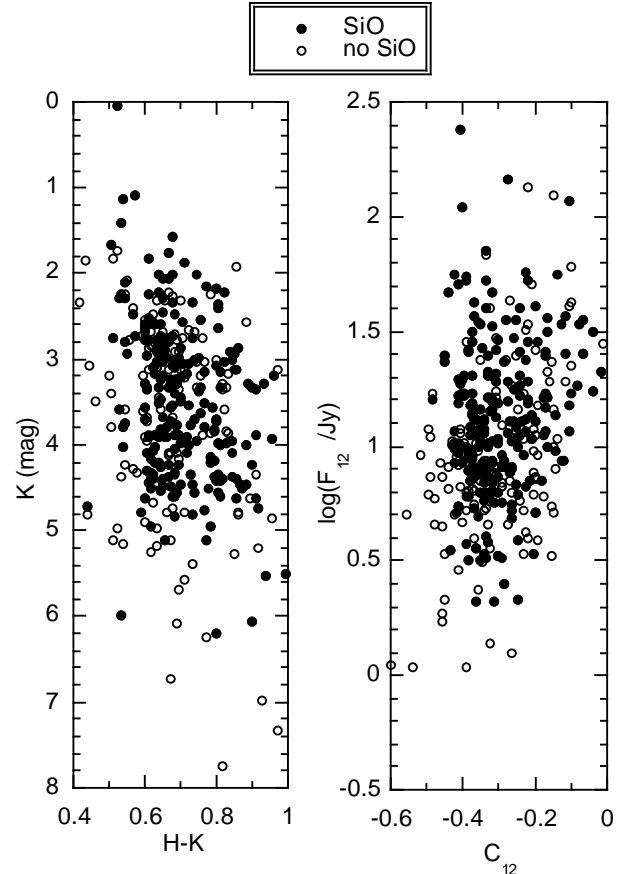


Fig. 2. NIR color-magnitude and MIR color-flux density diagrams for the sampled objects. Filled and unfilled circles indicate SiO detection and no detection, respectively.

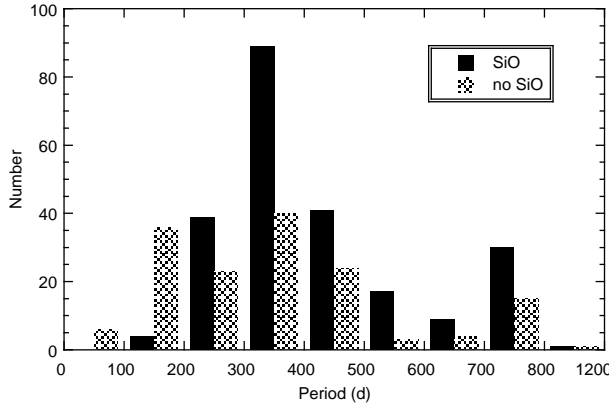


Fig. 3. Histogram of period for SiO detections and no detections. The filled and shaded areas indicate the SiO detection and no detection, respectively.

we can recognize that the present sample is weighted toward bluer colors than the previous SiO maser survey samples; for example, the median of $H - K$ for the present sample is 0.72, while it is 1.09 for the former sample, and the median of C_{12} in the present sample is -0.29 , while it is -0.16 for the former sample. In addition, the objects in the present sample are much brighter in K band than those in the previous samples. It suggests that the average distance from the Sun of the sampled stars is much smaller than that of the previous SiO-survey samples with a typical distance of ~ 4 kpc. The detection rate of SiO masers is quite high ($\sim 80\%$) for the objects that are bright in the $12\ \mu\text{m}$ and K bands, but gradually decreases as the infrared flux density decreases. Beyond $K = 5$, the number of no detections exceeds that of detections because of the large distance to the sources. Such a high SiO detection rate in SiO maser emission was an unexpected result, which apparently does not match up with the blue colors of the sample. However, this apparent discrepancy could be explained for the following reasons. In the previous SiO surveys, the variability indices of the IRAS catalog were not considered in the selection criteria (except Jiang et al. 1996). Therefore, the samples could include young stellar objects (YSOs) and red giants (RGB stars) which may mimic IR colors of the AGB stars, but do not emit SiO masers. On the contrary, the present sample is selected from the optically visible variable stars. It assures that they are stars in the AGB or post-AGB phases exhibiting active mass loss.

Figure 3 shows a histogram of period for the detections and no detections. The averaged period is $424 (\pm 158)$ d for the detections and $347 (\pm 192)$ d for the no detections, where the parenthetic number is a standard deviation. The SiO detection rate seems to increase with period, as has been found in the past surveys (e.g., see Figure 3 of Deguchi et al. 2004). We found 4 SiO maser sources with a period shorter than 200 d : J18424774+1548565, J19091839+7333285 (the shortest P=154 d), J20414535+3353226, and J22325976+6654394. All of them are semi-regulars. The blue miras with a pe-

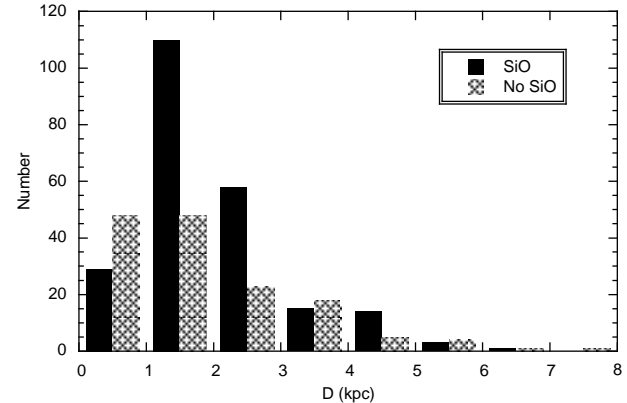


Fig. 4. Histogram of luminosity distances computed using the PL relation. The filled and shaded area indicates the SiO detection and non detection. The average distance is $2.0 (\pm 1.1)$ kpc for SiO detections and $2.2 (\pm 2.5)$ kpc for no detections, where the parenthetic number is a standard deviation.

riod less than 200 d occasionally exhibit a large deviant motion from the Galactic rotation (Feast & Whitelock 2000). However, above 4 objects (distributing in the Galactic longitude and latitude ranges of $l = 46 - 110^\circ$ and $b = -5 - +24^\circ$) spread only in the velocity range between -16 and $25\ \text{km s}^{-1}$. Therefore, we do not find any anomalous kinematics for these 4 objects only from their radial velocities.

We estimated distances to the observed stars based on the PL (Period-Luminosity) relation (Whitelock et al. 2008). The detail of the distance estimation is given in Appendix 2. Figure 4 shows histogram of distances for the detections and no detections. This figure indicates that most of objects in the sample are located within a distance of 3 kpc from the Sun except a few faint ones, though there is a considerable uncertainty in the distance estimation. The average distance is $2.0 (\pm 1.1)$ kpc for the detections, and $2.2 (\pm 2.5)$ kpc for the no detections.

3. Discussion

3.1. Longitude-velocity diagram

In Figure 5, we present the longitude-velocity diagram of the detections, in which filled and unfilled circles indicate the galactic latitude ranges of $|b| < 10^\circ$ and $|b| > 10^\circ$, respectively. Thick curves indicate the expected radial velocities for the objects under a circular rotation at distances, 1, 2, and 4 kpc from the Sun. Here we assumed a flat Galactic rotation curve of $220\ \text{km s}^{-1}$ in the Solar neighborhood and the Sun-Galactic-center distance of 8 kpc. We have also drawn the broken curves which are expected for the Hercules and Arcturus moving groups of stars near the Solar neighborhood (at the distance of 1 kpc). For simplicity, we assumed that the rotational lag and radial motion of the streams to the Galactic rotation are kept the same everywhere near the Solar neighborhood. The curve for each moving group strongly depends on the assumed velocity law: see, for example, Figure 8

and Appendix 3 of Deguchi et al. 2010).

In Figure 5, we see notable concentrations of the stars with $|b| < 10^\circ$ near the curve of 4 kpc distance; one around $l = 25 - 45^\circ$ and $V_{\text{lsr}} \simeq +40 - +80 \text{ km s}^{-1}$, and the other around $l = 95 - 135^\circ$ and $V_{\text{lsr}} \simeq -70 - -40 \text{ km s}^{-1}$. In addition, there is a group of stars in the area $l = 20 - 50^\circ$ and $V_{\text{lsr}} \simeq -80 - -20 \text{ km s}^{-1}$, which is deviant from the Galactic rotation by more than $\sim 50 \text{ km s}^{-1}$. These deviant groups of stars are surrounded by ellipses in Figure 6 for clarity. They are overlaid on the CO l - v map (Dame et al. 2001) for comparison.

The negative velocity feature around $l = 20 - 50^\circ$ ($V_{\text{lsr}} \simeq -80 - -20 \text{ km s}^{-1}$) has been discussed extensively by Deguchi et al. (2010). This is likely an extension of the Hercules moving group of stars, which is caused by outer Lindblad resonance of the Galactic bar structure. Bovy (2010) predicted that the member stars of the Hercules moving group would reveal most promisingly in the Galactic longitude range of $250^\circ \lesssim l \lesssim 290^\circ$. Unfortunately, stars in this longitude range are difficult to observe from Nobeyama except for stars at high Galactic latitudes. Furthermore, SiO maser sources (O-rich evolved stars) are not populated much outside the Solar circle (e.g., Jiang et al. 1996). Therefore, it is hard to confirm such a prediction through only the present discussion based on the longitude-velocity diagram.

3.2. Perseus group of deviant stars

One of notable characteristics of Figure 5 is that a considerable number of objects exhibit radial velocities larger than that expected from the 2 kpc distance; many stars fall around or beyond the curve of the 4 kpc distance. Because the objects in the present sample are optical variables which are bright in K band ($K < 4$), most of these are to be close to the Sun, i.e., their distances are smaller than 3 kpc. This discrepancy between the luminosity and kinematic distances is discussed below.

Figure 6 compares the distribution of the SiO sources with that of CO emission. The concentration of the points seen in the area of $l = 95 - 135^\circ$ and $V_{\text{lsr}} \simeq -70 - -40 \text{ km s}^{-1}$ coincides with a peak of CO emission feature for the Perseus spiral arm (see Dame et al. 2001). CO emission is most prominent at around $l = 111^\circ$ and $V_{\text{lsr}} = -45 \text{ km s}^{-1}$ (toward the NGC7538 molecular cloud). The average distance for the 18 objects in the ellipse of figure 5 (marked as Perseus) is estimated to be 1.94 kpc (with a standard deviation of $\pm 1.10 \text{ kpc}$) based on the period-luminosity (PL) relation. There is a large difference between the kinematic and luminosity distances for this group of stars. If we believe the luminosity distance, the stars of this group are approaching us with velocity larger than the velocity expected by the standard circular rotation of the Galaxy. Note that the SiO maser sources have a velocity dispersion of about 25 km s^{-1} from the average Galactic rotation [see the discussion in the last paragraph of Appendix 2 of Deguchi et al. (2005)].

The distance to the Perseus spiral arm was controversial in the past (Rickard et al. 1968; Roberts 1972). Recently parallax distances to the several maser objects

in this spiral arm have been measured with Very Long Baseline Interferometric (VLBI) technique. For example, the distance to W3(OH) ($l = 134^\circ$) is determined to be $1.95 \pm 0.04 \text{ kpc}$ (Xu et al. 2006). A comprehensive summary of the objects with annual parallax measurements is found in Figure 11 of Asaki et al. (2010), which visualizes positions and peculiar motions of several objects in this spiral arm. The Perseus spiral arm exhibits a systematic deviation from the circular rotation by a $\sim 30 \text{ km s}^{-1}$ in the longitude range $l = 90 - 150^\circ$. Since the 18 red variables toward the Perseus arm exhibit a similar kinematic characteristic, we conclude that these variables are associated with the Perseus spiral arm. An average period of the 18 red variables in the Perseus arm is 423 (± 109) d, which is longer than the average period of field optical miras of about 300 d (Whitelock et al. 2000; Templeton al. 2005). This fact indicates that they are relatively massive stars compared with the field miras. For example, the initial mass of AGB stars with $P=420 \text{ d}$ is about $2.5 M_\odot$ with age of 0.9 Gyr (see, e.g., Figure 20 of Vassiliadis & Wood 1993). Thus, the red variables in the Perseus arm has not left far from the birth place.

3.3. Sgr group of deviant stars

As well as the Perseus spiral arm, we may consider a possibility of association of another deviant group at $l = 25 - 45^\circ$ and $V_{\text{lsr}} \simeq +40 - +80 \text{ km s}^{-1}$ with the Sagittarius-Crux arm. The average distance and period of 21 stars in this group (the upper ellipse noted as Sgr group in Figure 6) are $2.58 (\pm 0.99) \text{ kpc}$ and $489 (\pm 160) \text{ d}$, respectively. Notable structures in this direction in our Galaxy are the Local Spur ($D \sim 0 - 2 \text{ kpc}$), the Sagittarius-Carina spiral arm ($D \sim 2 - 3 \text{ kpc}$), and the Scutum-Crux arm ($D \sim 3 - 5 \text{ kpc}$). It is possible that the Local Spur is a down stream branched from the Sagittarius-Crux arm. The branching to the Local spur seems to start near the tangent of the Sagittarius-Crux arm at $l \sim 55^\circ$.

In the l - v diagram (see the overlaid color map of figure 6), ^{12}CO emission is very weak around $(l, V_{\text{lsr}}) \sim (30^\circ, +60 \text{ km s}^{-1})$, except in the direction of the HII region G34.257 + 0.155. This is also true for the ^{13}CO map (Lee et al. 2001). The kinematic distance of the HII region G34.257 + 0.155 was estimated to be $3.8_{-0.8}^{+0.4} \text{ kpc}$ (Fish et al. 2003) from the HI absorption feature assuming the standard circular rotation. Recently the annual parallax distance was measured with VERA for the nearby infrared dark cloud, G034.43 + 00.24 (Kurayama, et al. 2011). The distance to the H_2O maser sources in this dark cloud is $\sim 1.56 \pm 0.12 \text{ kpc}$, which is considerably smaller than the kinematic distance of this cloud. Because the radial velocity of this cloud ($V_{\text{lsr}} \sim 50 - 60 \text{ km s}^{-1}$) is similar to that of the HII region G34.257 + 0.155, the distances of G34.257 + 0.155 may be overestimated. It is also likely that our deviant group of stars, which has a similar radial velocity in the same direction, is likely to be in the same spiral arm. Therefore, we call this group as the "Sgr" deviant group because the average luminosity distance of the stars in this deviant group is close to the estimated distance of the Sagittarius arm at $l \sim 30^\circ$.

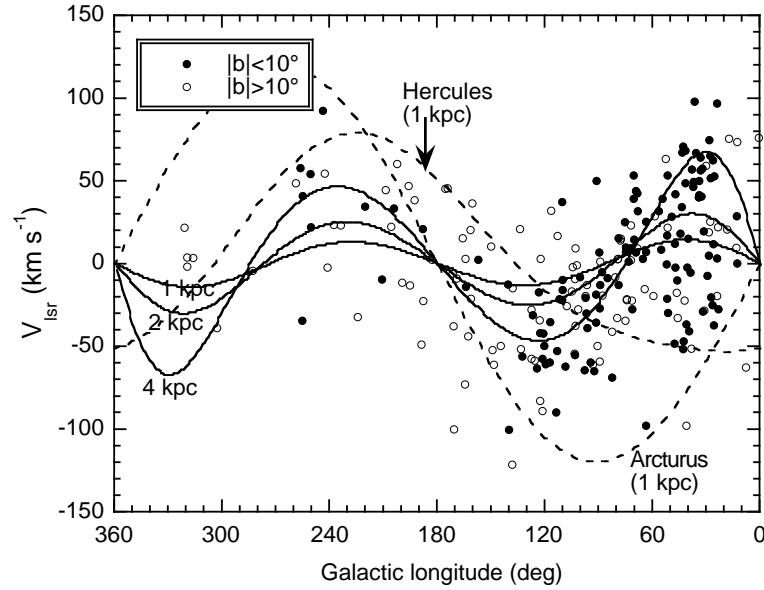


Fig. 5. Longitude-velocity diagram for SiO detected sources in the present sample. Filled and unfilled circles indicate objects below and above $|b| = 10^\circ$. Three thick curves indicate radial velocities expected from the model with a flat rotation curve of 220 km s $^{-1}$ for stars at distances 1, 2, and 4 kpc from the Sun, respectively. Broken curves indicate radial velocities expected for the Hercules and Arcturus moving groups of stars (with a rotational lag of -42 km s $^{-1}$ and an outward velocity of 52 km s $^{-1}$ for the Hercules group, and a rotational lag of -120 km s $^{-1}$ for the Arcturus group) at a 1 kpc distance from the Sun.

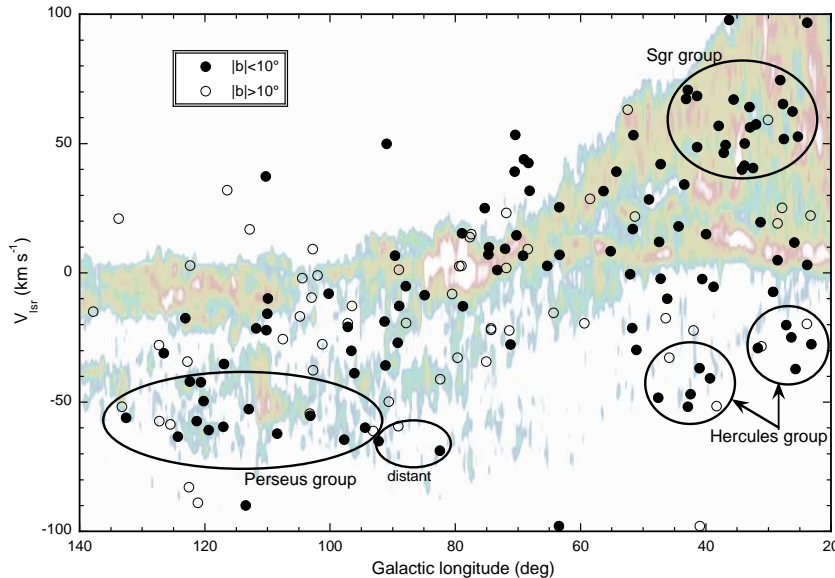


Fig. 6. A part of figure 5 but overlaid on the CO longitude-velocity map taken from Dame et al. (2001). Filled and unfilled circles indicate the SiO sources below and above $|b| = 10^\circ$. The large ellipses indicate the deviant groups of stars toward the Sagittarius and Perseus arms, and for the Hercules group of stars. Small ellipse assigned as "distant" indicates the distant stars which are not associated with the Perseus deviant group.

Reid et al. (2009) summarized the recent parallax measurements of massive star forming regions with VLBA and VERA by maser lines. Three star forming regions, G23.6–0.1, G35.2–0.7, and G35.2–1.7, exhibit the parallax distances in the range between 2 and 4 kpc in their table 4. However, one of these ($G23.6 - 0.1$) has a large radial velocity of $V_{\text{lsr}} = +83 \text{ km s}^{-1}$ (the kinematic distance $D_k^{\text{Std}} = 5.04 \text{ kpc}$ or $D_k^{\text{Rev}} = 4.77(\pm 0.3) \text{ kpc}$ for their new rotational parameters), but the parallax distance of this object is 3.19 kpc, which locates this object very near the far arm in this direction (the Scutum-Crux arm; see figure 5 of Reid et al. 2009). Another two source, G35.2–0.7 and G35.2–1.7, have much smaller radial velocities ($V_{\text{lsr}} = +28$ and $+42 \text{ km s}^{-1}$), for which the parallax distance roughly agrees with the kinematic distance (2 – 3 kpc). From these facts and the 1.6 kpc distance of the dark cloud $G034.43 + 00.24$ (Kurayama, et al. 2011), we conclude that the spiral arm in this direction has a complicated velocity structure and a large noncircular motion.

The exceeding velocity of the Sgr group of stars to the galactic rotation suggests either (1) that these stars move faster than the rotational velocity given by the flat rotation curve, or (2) that these stars move toward the galactic center (this inward motion causes the radial velocity increase in this direction). Because the directions of these two motions appear in opposite sense in the proper motion, VLBI observations of proper motions of objects in Sagittarius arm can be a good test of above cases.

Because the average period of this star group ($\sim 480 \text{ d}$) is considerably large compared with the average period of optical miras, they are relatively young objects compared with the field miras. Therefore it is likely that these stars are born in the Sagittarius arm and do not completely depart from this arm yet.

3.4. Correction in the distance for long-period miras

Optical and infrared properties of the candidates for the deviant groups are summarized in Table 5; it gives the 2MASS name, period, variability type, R magnitude, R amplitude of the variability, 2MASS K_s magnitude, error in the K magnitude, quality flag for the K magnitude, luminosity and kinematic distances. It involves a few stars with low photometric quality in the K band in the 2MASS catalog. These objects have relatively large distances compared with the average value of each group. Therefore the small average luminosity distances for these two groups of stars are not due to the objects with poor photometric accuracy.

In the previous sections, we used the PL relation which was derived from the photometric measurements of the miras with periods between 100 and 400 d (Whitelock et al. 2008), and extended the linear relation to the longer period up to 1000 d. However, it has been known that some miras with $P > 400 \text{ d}$, especially for OH/IR sources, lie above the linear extrapolation of the PL relation (e.g., see Feast 2009). This may cause an error in the distance estimation for the deviant group of stars. Therefore, we also applied the different PL relation for the stars with $P > 400 \text{ d}$, which was derived from the longer

Table 6. Distance statistics for the deviant groups of stars

Group (number)	Quantity	D_k (kpc)	D_L (kpc)	D_{Lc} (kpc)
Perseus (18)	average	5.27	1.94	2.19
	standard dev.	1.04	1.10	1.26
	<i>probability</i> [†]	—	$< 10^{-4}$	$< 10^{-4}$
Sgr (21)	average	3.63	2.58	3.45
	standard dev.	0.81	0.99	2.08
	<i>probability</i> [†]	—	$< 10^{-4}$	0.66
reduced Sgr (17)	average	3.46	2.26	2.65
	standard dev.	0.62	0.75	1.22
	<i>probability</i> [†]	—	$< 10^{-4}$	0.02

[†]: a probability of the Student's t-test for the averages of two sets of D_K and D_L (or D_K and D_{Lc}) being generated by the same distribution function.

period miras in the Large Magellanic Cloud (LMC) (Ita & Matsunaga 2011). The detail of this correction was described in Appendix 3. The corrected distances (applied for all of $P > 400 \text{ d}$ stars) are given in parenthetic number in the 8th column of Table 5. In this case, the average distance is $2.2 (\pm 1.3) \text{ kpc}$ for the Perseus group of stars, and it is $3.5 (\pm 2.1) \text{ kpc}$ for the Sgr group of stars, where the parenthetic number is the standard deviation. Therefore, such correction does not influence much for the distance estimation for the Perseus group, but it increases the average distance considerably for the Sgr group, because the latter group involves many stars with $P > 400 \text{ d}$. It is likely that the Sgr group of stars involve several very long period ($P = 730 \text{ d}$) stars, which contaminate this sample. If we remove the 4 stars with $P = 730 \text{ d}$, which is the upper boundary as a result of insufficient data in the NSVS survey (Williams et al. 2004), the average of the corrected luminosity distances of the Sgr group of 17 deviant stars is $2.6 (\pm 1.2) \text{ kpc}$. The average of the kinematic distances of this reduced set is $3.5 (\pm 0.7) \text{ kpc}$. The Student t-test gives a probability of 2 % for these two averages being produced by the same distribution function. In other words, with 98% confidence level, we can state that the average distances of these two sets are significantly different. In table 6, we summarized the average distance and standard deviation, and the t probability of the Student's t-test for the Perseus and Sgr (with smaller number) groups. In summary, the discrepancy between kinematic and luminosity distances for the Perseus and Sgr groups of stars are not removed by the correction in the distance for the $P > 400 \text{ d}$, though evidence is slightly weak for the case of the Sgr group.²

The present conclusion strongly depends on the luminosity distance based on the PL relation. Further examination on the accuracy of the distances will be given in the future paper, which also discuss the validity of the optical proper motions for these objects.

² Of course, the smaller sets using only the miras with $P < 400 \text{ d}$ give luminosity distances, $1.9 (\pm 1.2) \text{ kpc}$ and $1.8 (\pm 0.6) \text{ kpc}$ for the Perseus and Sgr groups, respectively. The difference between luminosity and kinematic distances is statistically significant in the Student's t-test for both groups, which are consistent with the previous result including the $P > 400 \text{ d}$ stars.

In this paper, we have given a preliminary analysis based on the obtained new radial velocities for a set of optical red variables, and have shown that they provide useful information on the kinematic of the stars in the Galaxy.

4. Summary

We have observed 379 red variables in the SiO maser lines, obtaining 229 (220 new) detections. Accurate radial velocities of the detected sources are used for investigating the kinematics of stars in the Solar neighborhood. Most of the observed stars locate within 3 kpc from the Sun according to luminosity distances. The longitude-velocity diagram of the sample shows high number densities of stars in two regions. The estimated luminosity distances suggest that these groups of stars spatially collocate with the Perseus and Sagittarius spiral arms. The result of the VLBI parallax measurements of the objects in these spiral arms seems to be consistent with the present data. However, at the current moment, the number of objects observed with VLBI is too small to conclude the membership of objects to the Galactic spiral arms except for the objects in the Perseus arm. In addition, we found a group of stars deviated by more than 40 km s^{-1} in a Galactic longitude range of $20\text{--}40^\circ$, which are likely to be members of the Hercules moving group. Proper motion data are essential to reveal the 3d motions of these stars, and the discussion based on the optically obtained proper motions will be given in a forthcoming paper.

We thank Dr. J. Nakashima, Univ. Hong Kong, for reading the manuscripts and useful comments. This research was partially supported by a Grant-in-Aid for Scientific Research from Japan Society for the Promotion of Sciences (20540234). This research made use of the SIMBAD and VizieR databases operated at CDS, Strasbourg, France, and as well as use of data products from Two Micron All Sky Survey, which is a joint project of the University of Massachusetts and Infrared Processing and Analysis Center/California Institute of Technology, funded by the National Aeronautics and Space Administration and National Science foundation.

Appendix. 1. SiO maser spectra and short notes on individual objects

We show the SiO maser spectra (the $J = 1\text{--}0$ $v = 1$ and 2 transitions) for detections in figures 8a–8m. We also show the spectra of other SiO maser transitions in figure 8. Individually interesting objects are noted as follows.

- *J02201452 + 7845362* (=AG Cep): This is a relatively bright IRAS source with $F_{12} = 34.1 \text{ Jy}$. H₂O maser emission has been detected at $V_{\text{lsr}} = 0.2 \text{ km s}^{-1}$ (Lewis 1997), which is considerably shifted from the SiO radial velocity $V_{\text{lsr}} = -28 \text{ km s}^{-1}$ measured in the present paper. OH maser searches have been negative (Nguyen-Q-Rieu et al. 1979; Lewis et al. 1995). The large velocity difference of about 30 km s^{-1} between H₂O and SiO maser lines suggests that this object is likely a water fountain source (Imai 2007). The central star, AG Cep, has a spectral type of M10, and a pulsation period of 403 d in the NSVS catalog, which is slightly different from the period of 445 d in the SVS catalog (Samus et al. 2010). The IRAS LRS spectra of this source exhibits a very sharp peak at $9.8 \mu\text{m}$ (LRS class 26), and Little-Marenin & Little (1990) classified the shape of silicate feature as "Sil+", which have high maser detection rate.
- *J01052742 + 6558594* (=V888 Cas): The IRAS LRS spectrum of this object (IRAS 01022+6542) was classified as C type (11 μm SiC feature; Volk et al. 1991), indicating a carbon star (Chen & Chen 2003). Searches for the 86.2 GHz SiO and 88.6 GHz HCN emissions with the IRAM 30m telescope were negative (Groenewegen et al. 2002). However, we detected SiO masers in this star at $V_{\text{lsr}} = -63 \text{ km s}^{-1}$. This result

suggests that the LRS feature is a silicate absorption at $10 \mu\text{m}$ typically seen in oxygen-rich evolved stars.

- *J03542359+1601019* (=UY Tau) and *J04212541+2015592* (V1110 Tau): These two stars have similar radial velocities, 45.5 and 45.2 km s^{-1} , respectively, at the same Galactic longitude $l = 175^\circ$. The data points for these two stars are overlapped in the longitude-velocity diagram (Figure 5), lying on the broken curve of the Hercules moving group. In fact, they are at high Galactic latitudes and separated by 8° in Galactic latitude ($b = -28.1$ and -20.5°). These two are likely members of the Hercules moving group.
- *J04402801 + 301650* (=V524 Aur): This is a medium bright IRAS source with $F_{12}=21.1 \text{ Jy}$ and IRAS LRS class of 13 (feature less), but this star has been slipped out from the past OH/IR and SiO maser surveys probably because of its "blue" MIR color ($C_{12} = -0.451$). The period of light variation of this star, 678 d, indicates that it is a considerably luminous and massive star among these objects. SiO masers have been detected for the first time in this paper. The observed SiO radial velocity ($V_{\text{lsr}} = -100.1 \text{ km s}^{-1}$) of this star at the Galactic coordinates of $(l, b) = (170.6^\circ, -10.7^\circ)$ indicates that this object is kinematically unusual.
- *J07314247+473226* (=DN Lyn): This star was once recorded as a dwarf nova and catalogued as a cataclysmic binary (Ritter & Kolb 2003). But this is in fact a faint mira (Kazarovets et al. 2002), and the status is corrected in the later version of the catalog of cataclysmic binaries [see on line version of Ritter & Kolb (2003)].³ This is a faint IRAS source ($F_{12} = 3.7 \text{ Jy}$), but SiO masers are detected at $V_{\text{lsr}} = -37.8 \text{ km s}^{-1}$ in the present paper.
- *J20125796+3214563* (=V557 Cyg): This star has an extreme radial velocity of $V_{\text{lsr}} = 53.4 \text{ km s}^{-1}$ at $l = 70.4^\circ$ in SiO masers. OH and H₂O masers have been detected for this star (Lewis et al. 1995). The longitude-velocity diagram (Figure 6) shows that several other stars also have similar (but slightly lower) radial velocities: *J20074663+3117241* ($V_{\text{lsr}} = 43.9 \text{ km s}^{-1}$) and *J20021291+3057556* ($V_{\text{lsr}} = 31.8 \text{ km s}^{-1}$). These three stars fall in a circle of 3 degree diameter, and the estimated distances are between 1.5 and 2.3 kpc (though the other two stars also fall near there in Figure 6, their distances are much larger). Because of their Galactic longitudes ($l \sim 70^\circ$), it is likely that these stars are not associated with the Sagittarius spiral arm. They move faster than the Galactic rotation by about 50 km s^{-1} .
- *J20195560+8816277* (=X UMi): This star is interesting for its location very near to the celestial north pole. We detected SiO masers at $V_{\text{lsr}} = -88.9 \text{ km s}^{-1}$; it is unusual as a star at the Galactic coordinates $(121.1^\circ, 26.5^\circ)$; see Figure 5. This star is located near the edge of the Polaris flare cloud in the local spur (Heithausen & Thaddeus 1990). The distance to this flaring cloud is not very far from the Sun, possibly less than 0.5 kpc ($V_{\text{lsr}} \sim -3 \text{ km s}^{-1}$). But this star is far away from the CO cloud because the distance is estimated to be 2.6 kpc. The pulsation period of this star is 338 d, and the 2MASS K_s magnitude is 4.3. IRAS 12 micron flux is 5.3 Jy with a color index $C_{12} = -0.37$. The spectral class is M8–9 (Gigoyan & Hambaryan 1996). Therefore, It is likely that this is a deviant star in the Perseus arm, but not a star in the Local spur.

Appendix. 2. Distance estimation using the Period–Luminosity relation

We estimated the luminosity distance from the observed K magnitudes using the Period-Luminosity (PL) relation (Whitelock et al. 2008),

$$M_K = -3.51 \times [\log(P) - 2.38] - 7.25. \quad (1)$$

³ <http://heasarc.gsfc.nasa.gov/W3Browse/all/rittercv.html>

The uncertainty of this formula is approximately 0.15 mag for the miras with a period between 150 and 400 d (Whitelock et al. 2008). The correction for stars with $P > 400$ d will be discussed in Appendix 3. The observed K magnitude can be corrected for the interstellar and circumstellar reddening (see equation (1) of Fujii et al. 2006)

$$K_c = K - A_K/E(H - K) \times [(H - K) - (H - K)_0], \quad (2)$$

where we use $A_K/E(H - K) = 1.44$ (Nishiyama et al. 2006), and $(H - K)_0$ is given by the empirical relation

$$(H - K)_0 = 0.420 \times \log(P) - 0.597 \quad (3)$$

(Catchpole 1992). Then, we can compute the distance from the difference between corrected and absolute K magnitudes, K_c and M_K , i.e.,

$$(D_L/\text{pc}) = 10^{0.2(K_c - M_K) + 1} \quad (4)$$

Figure 4 is a histogram of the derived distances using PL relation for the SiO detections and no detections. About 80% of the objects are at the luminosity distances below 3 kpc.

Accuracy of the obtained luminosity distance depends on two factors: reliability of the measured pulsation period and errors in the average K magnitude for a variable star. To check the reliability of the periods given by the NSVS catalog, we have cross-correlated the NSVS periods with those of the SVS catalog. Though the two periods derived from the NSVS and SVS catalogs coincide well for the medium-period objects ($P < 600$ d) in general, the coincidence becomes worse for the longer period stars. Therefore, we have to be careful to derive the distance based on the period given by the NSVS catalog. The present sample involves not only miras but semi-regulars too. Though 75 percent of stars in the present sample are of the variability type of mira, 20 percent of stars are of semi-regular type and 5 percent of stars are of other type (the latter two types are noted by symbols “†” and “‡” in the second column of table 4). Moreover, some miras with SiO masers occasionally exhibits a pulsation in a first overtone mode (Ita et al. 2006). Although it has been argued that semi-regulars may follow to a $P - M_K$ relation different from miras (for example, Bedding & Zijlstra 1998), the current understanding attributes this phenomenon to the multiplicity of pulsation modes (Tabur et al. 2010). For a certain percentage of stars with $P < 250$ d follows to the $P - M_K$ relation with almost the same slope but approximately one magnitude brighter than the standard sequence of the $P - M_K$ relation (sequence C in a $P - M_K$ diagram; Ita et al. 2004; Tabur et al. 2010). However, in the present analysis, we have used the single $P - M_K$ relation (1) for all of the observed stars, and estimated the distances. This is because it is hard to specify the pulsation mode for a particular star with $P < 250$ d whether or not it is of higher overtone modes. Fortunately, the SiO detection rate rapidly decreases for stars with a period below 250 d. Furthermore, semi-regulars have a low SiO detection rate ($\sim 13\%$ in the present semi-regular sample; see also Alcolea et al. 1990). In the present sample, only 18 stars with $P < 250$ d were detected in all the 229 SiO detections. Therefore, the error in the distance in the SiO detection sample is not severe. For the 18 Perseus group of stars, no semiregular was involved. For the 21 Sgr group of stars, one semiregular with $P = 351$ d, which is likely in the sequence C, was involved. Therefore, the multiplicity of the $P - M_K$ relation for the short period variables does not affect the discussions made in section 3.

The K-band amplitude of pulsation reaches to 0.8 magnitude for miras (Whitelock et al. 2008). The 2MASS K_s magnitude, which was measured at a single epoch, may differ from the average value in a pulsation period by about 1 mag [e.g., figure 11 of Messineo et al. 2004]. Furthermore for bright stars with $K < 4$, the 2MASS magnitude involves relatively large uncertainty (up to 0.4 mag) (Cutri et al. 2003). Therefore, we deduce that the derived luminosity distance may involve uncertainty of a factor of about 2 for individual objects. However, we expect that the uncertainty do not produce severe systematic shift in the distance scale and the average value for a certain number of stars is meaningful. Therefore, we believe that the uncertainty of the distance do not mislead the discussion made in the present paper.

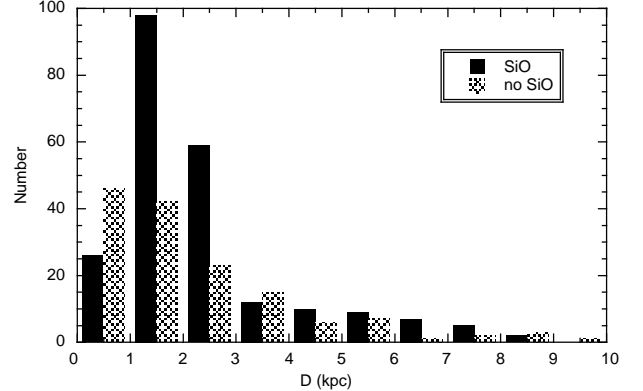


Fig. 7. Histogram of corrected luminosity distances computed using the PL relation (equation 5) for $P > 400$ d. The filled and shaded area indicates the SiO detection and non detection. The average distance is 2.4 (± 1.8) kpc for SiO detections and 2.8 (± 4.2) kpc for no detections, where the parenthetic number is a standard deviation.

Appendix. 3. Distance correction for the stars with $P > 400$ d.

It has been argued that the long-period variables with a period longer than 400 d lie systematically above a linear extrapolation of the PL relation of the miras with $100 < P < 400$ d [see a nice summary on this problem given by Feast (2009)]. Whitelock et al. (2003) concluded that all the luminous stars found by the early investigation of Hughes & Wood (1990) in the Large Magellanic Cloud (LMC) follow an extrapolation of the PL relation except a few stars under the Hot Bottom Burning (HBB) stage. Because Lithium is overabundant in many OH/IR (and SiO maser) stars (García-Hernández et al. 2007), it is very likely that the present sample of SiO maser sources is contaminated by the luminous HBB stars. Therefore, we re-estimated the distances of stars introducing the PL relation with a steeper gradient at $P > 400$ d. We use for stars with $P > 400$ d,

$$M_K = -6.850 \times [\log(P) - 2.6] - 8.406, \quad (5)$$

and

$$(H - K)_0 = 1.271 \times [\log(P) - 2.6] + 0.271. \quad (6)$$

These equations are derived based on the JHK band observations of the long period variables in the range $2.6 < \log(P) < 2.95$ in the LMC (Ita & Matsunaga 2011). The apparent H and K magnitudes in LMC are converted to M_K with a distance modulus of 18.5 for LMC. Because the circumstellar extinction is negligibly small for these LMC O-rich stars at $\log(P) < 2.95$ in their study, the linear fits of H and K against $\log(P)$ in their paper represent the H and K magnitudes without extinction. Therefore, the difference between the H and K linear fits directly gives $(H - K)_0$. The uncertainty of the linear fit in K is deduced to be about 0.36 mag (if we assume the deviation in K is the same as that in the LMC; Ita & Matsunaga 2011). From the above equations, we can compute the final correction factor for the distance for the stars with $P > 400$ d as

$$D_{Lc}/D_L = 10^{0.913 \times [\log(P) - 2.6]}. \quad (7)$$

where D_{Lc} and D_L are the corrected luminosity distance for $P > 400$ d and the luminosity distance given in Appendix 2 (equation 1), respectively. The correction factor increases up to about a factor of 2 for $P = 850$ d. We gave the corrected distance for the Perseus and Sgr groups of stars in parenthetic number at the 9th column of table 5. The histogram of the luminosity distances in the present sample, which is corrected for all of the $P > 400$ d stars, is shown in Figure 7.

The PL relation for the $P < 400$ d stars does not exhibit a significant offset between the LMC and our Galaxy (Whitelock et al. 2008). Therefore it is reasonably expected that, for the longer period stars ($P > 400$ d), the same relation holds both in the LMC and in our Galaxy, except for a special environment such as the Galactic center (e.g., Ortiz et al. 2002).

References

- Alcolea, J., Bujarrabal, V., & Gomez-Gonzalez, J. 1990, A&A, 231, 431
- Asaki, Y., Deguchi, S., Imai, H., Hachisuka, K., Miyoshi, M. & Honma, M. 2010, ApJ, 721, 267
- Bedding, T. R. & Zijlstra, A. A. 1998, ApJ, 506, L47
- Beichman, C. et al., 1989, NASA RP-1190 "IRAS Point Source Reject Catalog"
- Belokurov, V. et al. 2007, ApJ, 657, L89
- Bensby, T., Oey, M. S., Feltzing, S., & Gustafsson, B. 2007, ApJ, 655, L89
- Benson, P. J. & Little-Marenin, I. R. 1996, ApJS, 106, 579
- Bovy, J., 2010, arXiv1006.0736B
- Catchpole, R. 1992, ASPC, 30, 295
- Chen, P.-S. & Chen, W.-P. 2003, AJ, 125, 2215
- Cho, S.-H. & Kim, J. 2010, ApJ, 719, 126
- Cho, S., Kaifu, N., & Ukita, N. 1996, AJ, 111, 1987
- Crocker, D. A. & Hagen, W. 1983, A&AS, 54, 405
- Cutri, R.M., et al. 2003, 2MASS All Sky Catalog of Point Sources⁴
- Dame, T. M., Hartmann, D. & Thaddeus, P. 2001, ApJ, 547, 792
- Deguchi, S., Fujii, T., Izumiura, H., Kameya, O., Nakada, Y., & Nakashima, J. 2000, ApJS, 130, 351
- Deguchi, S., Fujii, T., Ita, Y., Imai, H., Izumiura, H., et al. 2007, PASJ, 59, 559
- Deguchi, S., Imai, H., Fujii, T., Glass, I., Ita, Y. et al. 2004, PASJ, 56, 261
- Deguchi, S., Nakashima, J., Miyata, T., & Ita, Y. 2005, PASJ, 57, 933
- Deguchi, S., Shimoikura, T., & Koike, K. 2010, PASJ, 62, 525
- Eder, J., Lewis, B. M., & Terzian, Y. 1988, ApJS, 66, 183
- Egan, M. P., Price, S. D., Kraemer, K. E., Mizuno, D. R., Carey, S. J., et al. 2003, Air Force Research Laboratory Technical Report AFRL-VS-TR-2003-1589
- Eggen, O. J. 1996, AJ, 112, 1595
- Engels, D. & Lewis, B. M. 1996, A&AS, 116, 117
- Engels, D., Schmid-Burgk, J. & Walmsley, C. M. 1988, A&A, 191, 283
- Famaey, B., Jorissen, A., Luri, X., Mayor, M., Udry, S., Dejonghe, H., & Turon, C. 2005, A&A, 430, 165
- Feast, M. W. 2009, asrp.proc, 48 (arXiv:0812.0250)
- Feast, M. W. & Whitelock, P. A. 2000, MNRAS, 317, 460
- Fish, V. L., Reid, M. J., Wilner, D. J. & Churchwell, E. 2003, ApJ, 587, 701
- Fujii, T., Deguchi, S., Ita, Y., Izumiura, H., Kameya, O., Miyazaki, A., & Nakada, Y. 2006, PASJ, 58, 529
- Galt, J. A., Kwok, S., & Frankow, J. 1989, AJ, 98, 2182
- García-Hernández, D. A., García-Lario, P., Plez, B., Manchado, A., D'Antona, F., Lub, J., & Habing, H. 2007, A&A, 462, 711
- Gigoyan, K. S. & Hambaryan, V. V. 1996, Astrophysics, 39, 310
- Groenewegen, M. A. T., Sevenster, M., Spoon, H. W. W., Pérez, I. 2002, A&A, 390, 501
- Haikala, L. K., Nyman, L.-Å., & Forsström, V., 1994, A&AS, 103, 107
- Hall, P. J., Allen, D. A., Troup, E. R., Wark, R. M., & Wright, A. E., 1990, MNRAS, 243, 480
- Heithausen, A. & Thaddeus, P. 1990, ApJ, 353, L49
- Hughes, S. M. G. & Wood, P. R. 1990, AJ, 99, 784
- Imai, H. 2007, IAUS, 242, 279
- Ita, Y., & Matsunaga, N. 2011, MNRAS, 412, 2345
- Ita, Y., Deguchi, S., Fujii, T., Kameya, O., Miyoshi, M., Nakada, Y., Nakashima, J., & Parthasarathy, M. 2001, A&A, 376, 112
- Ita, Y., Tanabé, T., Matsunaga, N., Nakajima, Y., Nagashima, C. et al. 2004, MNRAS, 347, 720
- Ita, Y., Deguchi, S., Matsunaga, N. & Fukushi, H. 2006, Mem. Soc. Astr. Italy, 77, 85
- Izumiura, H., Deguchi, S., Hashimoto, O., Nakada, Y., Onaka, T., Ono, T., Ukita, N., & Yamamura, I. 1995, ApJ, 453, 837
- Jewell, P.R., Snyder, L.E., Walmsley, C.M., Wilson, T.L., Gensheimer, P.D. 1991, A&A 242, 211
- Jiang, B.W., Deguchi,S., & Ramesh, B. 1999, PASJ, 51, 95
- Jiang, B. W., Deguchi, S., Yamamura, I., Nakada, Y., Cho, S. H., & Yamagata, T. 1996, ApJS, 106, 463
- Kazarovets, E.V., Samus, N.N., Durlevich, O.V. 2002, IBVS, 5135, 1
- Kim, J., Cho, S.-H., Oh, C. S., Byun, D.-Y. 2010, ApJS, 188, 209
- Kobayashi, H., Kawaguchi, N., Manabe, S., Shibata, K. M., Honma, M. et al. 2008, IAUS, 248, 148
- Kurayama, T., Nakagawa, A., Sawada-Satoh, S., Sato, K., Honma, M., Sunada, K., Hirota, T., & Imai, H. 2011, arXiv1102.2056K
- Lee, Y., Stark, A. A., Kim, H-G., Moon, D-S., 2001, ApJS, 136, 137
- Lewis, B. M. 1994, ApJS, 93, 549
- Lewis, B. M. 1997, AJ, 114, 1602
- Lewis, B. M. & Engels, D. 1988, Nature, 332, 49
- Lewis, B. M., Eder, J. & Terzian, Y. 1990, ApJ, 362, 634
- Lewis, B. M., David, P., & Le Squeren, A. M. 1995, A&A, 111, 237
- Little-Marenin, I. R., & Little, S. J. 1990, AJ, 99, 1173
- Majewski, S. R., Skrutskie, M. F., Weinberg, M. D., Ostheimer, J. C. 2003, ApJ, 599, 1082
- Messineo, M., Habing, H. J., Menten, K. M., Omont, A. & Sjouwerman, L. O. 2004, A&A, 418, 103
- Nakashima, J. & Deguchi, S. 2003, PASJ, 55, 203
- Nakashima, J. & Deguchi, S. 2006, ApJL, 647, L139
- Nguyen-Q-Rieu, Laury-Micoulaut, C., Winnberg, A., & Schultz, G. V. 1979, A&A, 75, 351
- Nishiyama, S., Nagata, T., Kusakabe, N., Matsunaga, N., & Naoi, T. 2006, ApJ, 638, 839
- Olonon, F. M., & IRAS Science team, 1986, A&AS, 65, 607
- Ortiz, R., Blommaert, J.A.D.L., Copet, E., Ganesh, S., Habing, H.J., et al. 2002, A&A, 388, 279
- Parimucha, Š, 2003, Contri. Astron. Obs. Ska. Pleso, 33, 99
- Pojmanski et al. 2005, "ASAS Variable Stars in Southern hemisphere (Pojmanski+, 2002-2005)", on line catalog available at VizieR
- Reid, M. J., Menten, K. M., Zheng, X. W., Brunthaler, A., Moscadelli, L., et al. 2009, ApJ, 700, 137
- Rickard, J. J. 1968, ApJ, 152, 1019
- Ritter, H. & Kolb, U. 2003, A&A, 404, 301 and see online catalog: version 7.14⁵

⁴ <http://irsa.ipac.caltech.edu/applications/Gator/>

⁵ <http://physics.open.ac.uk/RKcat/> .

- Roberts, W. W., Jr. 1972, ApJ, 173, 259
- Roeser, S., Demleitner, M., & Schilbach, E. 2010, AJ, 139, 2440
- Samus N.N., Durlevich O.V., et al. 2010, "Catalog of Variable Stars (GCVS database, Version 2010Jan)" available in VizieR
- Scholz, M. & Wood, P. R. 2000, A&A, 362, 1065
- Sevenster M.N., van Langevelde, H. J., Moody, R. A., Chapman J.M., Habing H.J., & Killeen, N.E.B., 2001, A&AS, 366, 481
- Sjouwerman, L. O., Capen, S. M., & Claussen, M. J. 2009, ApJ, 705, 1554
- Tabur, V., Bedding, T. R., Kiss, L. L., Giles, T., Derekas, A., & Moon, T. T. 2010, MNRAS, 409, 777
- Templeton, M. R., Mattei, J. A., Willson, L. A. 2005, AJ, 130, 776
- van Blerkom, D. & Mao, X. 1982, ApJL, 252, L73
- van der Veen, W. E. C. J., & Habing, H. J. 1988, A&A, 194, 125
- Vassiliadis, E., & Wood, P. R. 1993, ApJ, 413, 641
- Volk, K., Kwok, S., Stencel, R. E., & Brugel, E. 1991, ApJS, 77, 607
- Whitelock, P., Marang, F., & Feast, M. 2000, MNRAS, 319, 728
- Whitelock, P. A., Feast, M., W., van Loon, J. T., Zijlstra, A. A. 2003, MNRAS, 342, 86
- Whitelock, Patricia A., Feast, M. W. & van Leeuwen, F. 2008, MNRAS, 386, 313
- Williams, P.R., Woźniak, S.J., Vestrand, W.T., & Gupta, V. 2004, AJ, 128, 2965
- Woźniak, P. R., Williams, S. J., Vestrand, W. T., & Gupta, V. 2004, AJ, 128, 2965
- Xu, Y., Reid, M. J., Zheng, X. W. & Menten, K. M. 2006, Sci. 311, 54
- Zuckerman, B. 1979, ApJ, 230, 442
- Zwitter, T., Siebert, A., Munari, U., Freeman, K. C., Siviero, A. et al. 2008, AJ, 136, 421Z

**A full version of this paper including Figure 8a–8m, and Figure 9 (SiO maser spectra for detections) are available at
http://www.nro.nao.ac.jp/~lib_pub/report/data/no680.pdf.**

Table 1. Observational results of SiO Masers.

2MASS name (J—)	SiO $J = 1-0$ $v = 1$ maser line				SiO $J = 1-0$ $v = 2$ maser line				rms (K) (yymmdd)	obs. date
	T_a (K)	V_{lsr} (km s $^{-1}$)	L.F. (K km s $^{-1}$)	rms (K)	T_a (K)	V_{lsr} (km s $^{-1}$)	L.F. (K km s $^{-1}$)	rms (K)		
00100914+5452343	0.403	-34.6	0.950	0.062	0.415	-35.9	1.695	0.068	100225	
00163648+6601104	0.283	-60.9	0.539	0.058	0.249	-60.5	0.444	0.056	090309	
00202547+6947567	0.617	-49.5	2.026	0.082	0.938	-49.6	2.752	0.094	100225	
00251001+7008516	1.195	-43.3	5.694	0.057	1.365	-41.3	4.394	0.067	100225	
00365942+6308016	2.428	-58.5	11.692	0.143	2.297	-56.0	12.320	0.139	090308	
00382283+8021250	0.340	2.9	0.639	0.074	—	—	—	0.076	100321	
00452805+7550219	0.607	-83.1	1.998	0.058	0.438	-82.6	1.883	0.065	100225	
00480999+5334010	—	—	—	0.051	0.244	-42.0	0.307	0.063	100225	
00504329+4630307 [†]	1.792	-34.3	5.293	0.098	1.480	-34.1	4.131	0.101	100222	
00532514+6501559	1.173	-15.5	4.471	0.131	0.946	-19.2	3.701	0.115	090308	
01052742+6558594	0.952	-62.9	4.308	0.104	0.671	-63.8	2.265	0.097	090308	
01070453+4924467 [†]	0.752	-58.9	3.451	0.066	0.988	-58.0	4.119	0.068	100222	
01215470+6120551	0.565	-30.4	1.477	0.053	0.604	-31.6	1.591	0.061	100412	
01564706+3401107	1.001	-120.9	1.999	0.074	0.648	-121.9	1.579	0.085	100227	
02055459+4043267	0.413	-19.9	1.665	0.049	0.472	-9.9	1.553	0.052	100222	
02201452+7845362	1.017	-28.0	1.835	0.082	1.210	-27.7	1.629	0.086	100222	
02304255+6635004	0.000	0.0	0.000	0.049	0.243	-56.0	0.382	0.053	100412	
02431547+8108095	1.692	-57.3	4.144	0.096	1.591	-57.2	3.627	0.099	100222	
02444549+1219029	0.841	20.5	2.257	0.081	0.392	20.2	0.677	0.101	100227	
02522580+3641298	0.714	-60.9	1.990	0.089	0.540	-61.0	3.107	0.091	100412	
02561803+4553132	0.409	-47.4	1.436	0.052	0.199	-52.1	0.682	0.057	100222	
02572747+1118057	1.717	15.4	4.300	0.088	0.949	15.4	1.500	0.098	100227	
03043767+5649144	0.241	-12.4	1.296	0.040	0.190	-12.5	0.795	0.043	100222	
03194960+6120515	0.812	-100.1	1.602	0.100	0.653	-100.5	1.141	0.103	100412	
03323218+7427045	1.017	-50.8	2.744	0.132	1.353	-52.6	5.042	0.153	100412	
03483231+3216437	1.097	-21.3	2.872	0.123	0.821	-20.8	1.821	0.121	100302	
03542359+1601019	0.742	46.0	2.751	0.092	0.545	45.1	1.080	0.103	100227	
04153489+3349461	0.674	-71.9	2.460	0.119	1.587	-73.9	4.153	0.125	100302	
04212541+2015592	1.362	44.7	4.059	0.106	1.773	45.7	5.831	0.124	100227	
04232410+0634322	1.908	-22.6	2.849	0.183	1.529	-22.6	2.071	0.162	090506	
04341277+4715357	0.457	2.4	1.050	0.070	1.062	2.4	2.651	0.072	100222	
04355719+2830524	5.954	-5.8	12.520	0.286	4.796	-5.9	5.642	0.116	080426	
04402801+3016500	1.582	-100.0	4.241	0.100	1.521	-100.2	4.551	0.106	100405	
04505728+0308323	0.213	-16.3	0.659	0.059	0.241	-10.1	0.954	0.065	100405	
04553028+0304281	0.331	47.6	0.692	0.067	0.729	46.5	1.891	0.063	101208	
05001777+6046152	0.320	-50.3	2.252	0.054	0.906	-54.1	2.304	0.058	100222	
05381725+4700121	0.312	-13.7	0.894	0.067	0.752	-14.1	1.973	0.070	100222	
05413366-0407549	0.755	44.4	2.196	0.092	—	—	—	0.094	100302	
05435348+0310111	2.670	60.4	11.206	0.125	0.178	60.3	8.894	0.129	100302	
05490636-3220002	0.755	23.5	2.755	0.096	0.930	23.5	1.887	0.093	101209	
05505493+0018131	3.375	22.3	7.697	0.130	2.118	22.3	5.993	0.129	100302	
05572394+4822417 [†]	8.095	2.9	22.679	0.088	9.455	2.9	22.782	0.090	100222	
05581447+5002407 [†]	0.795	-43.3	3.205	0.076	2.214	-44.3	6.295	0.081	100222	
06015218+2149051	0.351	21.8	1.249	0.087	0.626	20.3	2.347	0.089	100302	
06340951-1017085	—	—	—	0.056	0.222	34.4	0.773	0.048	101209	
06450560+0902184	1.104	33.1	4.552	0.087	1.380	33.7	3.102	0.090	100222	
06570903+4735220	0.456	-10.8	1.824	0.055	0.307	-7.2	0.561	0.056	100222	
06574519+0318093	0.674	-8.6	3.260	0.092	1.322	-10.3	5.514	0.099	100223	
07072185+2817559	4.483	-49.0	14.031	0.087	3.922	-48.5	11.262	0.092	100223	
07073432+2413190	0.536	38.6	2.615	0.074	0.761	38.3	1.096	0.074	100223	
07100587+6556246	1.984	10.3	6.786	0.071	3.262	10.4	7.784	0.075	100222	
07125372+1739161	1.758	-11.5	5.007	0.109	1.321	-11.5	2.561	0.102	090321	
07314247+4733226	0.206	-37.5	0.504	0.063	0.527	-38.1	1.077	0.066	100222	
07553633-3936228 ¹	0.816	40.9	3.805	0.120	1.741	40.8	4.866	0.136	100225	
07555070+5711533	1.458	36.5	7.553	0.066	0.697	36.5	3.342	0.070	100222	
08093981-3810285 ¹	0.995	-34.4	2.712	0.134	1.173	-34.7	2.465	0.146	100225	
08102916-3247207	0.312	50.0	0.931	0.076	0.351	58.3	1.300	0.074	100225	
08170543-3126193	1.539	21.2	5.461	0.103	1.558	22.9	3.947	0.108	100225	
08254033-2210342	0.284	88.2	0.550	0.056	0.202	96.8	0.580	0.051	101207	
08355329-1911284	0.545	53.6	1.115	0.071	0.239	55.1	0.701	0.075	100314	
08400691-0813472	0.643	22.7	2.560	0.068	0.709	23.6	1.934	0.070	100222	
08414614+0211202	0.679	-32.2	1.868	0.088	1.241	-32.5	3.048	0.094	100222	
08520560-3305439	3.507	57.7	11.490	0.119	1.377	58.1	4.229	0.129	100225	
09243332-3043520	0.512	49.3	1.785	0.071	0.523	48.1	2.180	0.078	100225	
09422273+7751074	4.430	21.1	9.394	0.089	2.436	21.1	4.737	0.096	100222	
09572218-0232555	0.767	-2.9	2.626	0.082	1.226	-1.9	3.188	0.086	100223	

Table 1. (Continued.)

2MASS name (J—)	SiO $J = 1-0$ $v = 1$ maser line				SiO $J = 1-0$ $v = 2$ maser line				rms (K)	obs. date (yymmdd.d)
	T_a (K)	V_{lsr} (km s $^{-1}$)	L.F. (K km s $^{-1}$)	rms (K)	T_a (K)	V_{lsr} (km s $^{-1}$)	L.F. (K km s $^{-1}$)	rms (K)		
11353071+3452042	0.663	3.4	1.240	0.092	1.695	1.7	2.022	0.118	080410	
12002079-1011049	1.488	-4.3	1.573	0.075	0.490	-4.3	1.571	0.080	100223	
12505315-2950431	0.432	-38.5	1.913	0.084	0.684	-39.6	2.076	0.090	100223	
13512546-3656376	3.925	3.7	14.801	0.123	1.939	3.4	6.004	0.127	100223	
13564515-2532429	0.664	20.9	1.300	0.090	1.105	22.8	2.438	0.101	100223	
13574319-3104110	0.863	-1.4	1.899	0.095	0.907	-2.2	1.832	0.103	100223	
14045992-3529505 ^{†,8}	13.408	3.6	30.051	0.139	5.267	4.2	12.666	0.135	100223	
16385186+1403583	0.527	-27.7	1.536	0.049	0.790	-28.9	1.698	0.082	050523	
16510590+1020515 ²	0.878	20.6	4.080	0.103	0.743	17.7	2.781	0.102	100512	
16523612-0527277	0.391	19.1	0.415	0.078	—	—	—	0.090	100516	
16582342-2054105	0.245	76.1	0.771	0.065	0.246	75.9	0.204	0.060	100315	
16584672-1243469	0.413	-60.8	1.273	0.056	0.203	-64.6	0.629	0.055	100315	
16594972+5219044	0.239	-31.6	0.316	0.032	0.213	-33.7	0.390	0.040	101220	
17040522+7147470	0.476	-54.2	1.396	0.073	0.425	-54.6	0.977	0.086	100225	
17192766-1015403	0.458	73.9	1.171	0.080	0.345	73.1	0.941	0.080	100315	
17253651+0111059	0.620	-20.6	3.067	0.077	0.529	-18.5	2.760	0.080	080427	
17272100-0613166	0.338	73.6	1.261	0.063	0.305	77.5	0.629	0.059	100315	
17280830+0502185	1.654	25.3	2.290	0.118	0.793	25.2	1.637	0.104	100315	
17381195-1241572	0.480	28.7	2.172	0.077	0.328	28.5	1.026	0.080	100315	
17392120-1312145	0.406	0.2	1.321	0.083	—	—	—	0.082	100516	
17424879-0146555	0.209	22.6	1.127	0.056	0.187	21.7	0.544	0.053	100315	
17444713+5437173	1.632	-40.2	5.571	0.138	0.813	-41.7	2.708	0.138	100428	
17445378+2129466	0.500	-32.7	0.752	0.101	1.170	-32.9	1.860	0.099	100512	
18032344-0218030	0.000	0.0	0.400	0.093	0.505	52.8	0.818	0.083	100315	
18050458+0246114	0.558	58.2	1.854	0.080	0.552	60.1	0.979	0.077	100315	
18074103-0518196	0.501	-27.5	1.023	0.089	0.342	-27.4	0.918	0.082	100315	
18154122-0331121	0.360	-37.2	1.104	0.074	—	—	—	0.072	100512	
18223780+0637444	1.603	67.9	5.216	0.102	1.225	66.3	4.000	0.083	100405	
18230711-0146024	1.571	74.6	3.409	0.110	0.890	74.6	2.618	0.110	100315	
18230994-0636023	0.613	2.2	1.896	0.096	0.505	4.1	1.552	0.091	100315	
18234044-0421328	0.562	10.2	2.424	0.116	0.953	13.4	2.276	0.112	100512	
18250094-0650575	1.824	95.4	5.831	0.109	0.665	98.1	3.036	0.104	100512	
18260088+5055498	0.181	1.9	0.423	0.046	0.230	3.4	0.450	0.049	101220	
18272417-0100456 [†]	2.039	-7.2	8.219	0.151	1.593	-7.5	5.898	0.133	100315	
18274054+4918331	0.575	13.4	1.235	0.105	0.345	14.5	0.479	0.104	100428	
18285243+0150161	0.516	58.9	2.716	0.082	0.467	56.0	1.854	0.083	100315	
18335184+0342484	0.238	36.2	0.496	0.044	0.392	44.0	1.733	0.045	100405	
18361528+0126242	0.526	40.5	1.068	0.098	0.994	40.7	1.846	0.097	100316	
18371700+0615306	1.151	49.6	3.724	0.132	0.922	49.5	3.674	0.126	100512	
18373693+1309559	0.788	67.5	1.104	0.129	1.565	67.1	3.010	0.117	100512	
18391722-0320102 ³	1.054	4.9	3.483	0.110	1.033	5.1	3.583	0.108	090307	
18395233-0423328	0.445	65.6	1.363	0.074	0.618	65.2	1.751	0.086	100526	
18401649+0004131	0.195	-29.1	0.308	0.066	0.352	-28.9	0.752	0.068	100526	
18420997+1038548	1.633	68.3	3.794	0.087	0.569	68.4	1.943	0.090	100511	
18422141+0208504	0.765	48.4	2.092	0.098	0.614	51.7	2.750	0.101	100511	
18424774+1548565	—	—	—	0.087	0.491	-10.0	1.491	0.085	100512	
18440224-0638441	0.496	65.8	1.461	0.094	0.560	59.1	1.623	0.091	090307	
18451727+0056300	0.391	63.9	0.961	0.062	0.421	64.6	0.728	0.057	090307	
18473513-0651009	0.326	-25.8	0.706	0.076	0.377	-24.0	0.796	0.081	100511	
18482850-0540524	0.845	52.6	3.140	0.083	1.142	51.0	4.710	0.091	101220	
18533423+0048559	0.231	42.6	1.022	0.048	0.304	40.4	0.440	0.052	101220	
18541840-0648564 [†]	2.358	-20.2	7.748	0.133	2.306	-20.3	7.452	0.131	100511	
18550405+0606293	0.469	-5.2	2.319	0.082	0.702	-5.7	2.222	0.079	090307	
18551284+1041470	0.980	-51.8	3.819	0.157	2.276	-51.5	4.940	0.201	100511	
19013031+0954055	0.265	71.2	0.736	0.057	0.254	70.4	0.438	0.057	090307	
19021502+4712597	0.381	15.1	0.448	0.084	—	—	—	0.079	100428	
19030960-0128366	0.410	56.3	1.543	0.077	0.502	56.3	1.536	0.073	100512	
19042996+0305134	0.635	42.4	2.166	0.069	0.270	50.6	1.320	0.070	101220	
19084758-0402461	0.488	20.2	1.567	0.081	0.538	19.0	1.386	0.076	100315	
19091839+7333285	0.216	-16.3	0.651	0.057	0.256	-17.2	0.750	0.069	100506	
19092954+0127514	0.340	97.6	0.604	0.062	0.200	98.1	0.450	0.060	100315	
19145099+0414308	1.595	-40.8	8.324	0.135	1.645	-40.6	4.599	0.134	051222	
19145678+2204305	2.493	7.5	17.230	0.119	2.393	9.4	13.686	0.117	100420	
19152147+0233020	0.400	55.5	0.814	0.096	0.426	58.2	1.445	0.095	051222	
19154874+0945208	0.660	18.0	1.419	0.103	0.728	18.2	1.047	0.111	100420	

Table 1. (Continued.)

2MASS name (J—)	SiO $J = 1-0$ $v = 1$ maser line				SiO $J = 1-0$ $v = 2$ maser line				rms (K)	obs. date (yyymmdd.d)
	T_a (K)	V_{lsr} (km s $^{-1}$)	L.F. (K km s $^{-1}$)	rms (K)	T_a (K)	V_{lsr} (km s $^{-1}$)	L.F. (K km s $^{-1}$)	rms (K)		
19161015+0841001	0.208	33.0	0.773	0.055	0.117	35.6	0.155	0.050	090307	
19163390+1822517	0.586	-2.2	1.945	0.115	1.239	1.3	2.458	0.111	100315	
19170076+1456093	0.362	28.9	0.520	0.069	0.281	28.2	0.726	0.075	090307	
19172579+4248497	0.828	-21.8	2.975	0.084	0.533	-21.0	1.782	0.085	100518	
19195583+1254351	1.188	-48.2	1.283	0.117	0.753	-48.2	2.295	0.121	090307	
19202271+0455507	0.781	-3.2	1.275	0.114	1.170	-1.4	3.499	0.122	090308	
19221604+0506593	1.762	-37.4	4.993	0.103	1.635	-36.2	4.579	0.100	100511	
19242261+3219082	0.358	1.9	1.921	0.085	0.744	3.8	2.158	0.096	100506	
19252049+0620243	0.336	-45.1	1.443	0.062	0.429	-48.6	2.146	0.063	090308	
19261909+1640323 [†]	1.358	18.2	10.827	0.113	1.833	15.8	9.539	0.106	090308	
19265263+1644068	1.808	-21.2	8.768	0.118	2.368	-21.4	6.891	0.119	100511	
19271451+1129045	3.638	42.3	13.952	0.102	2.539	41.9	9.405	0.098	090308	
19273109+1928141	1.048	40.6	3.276	0.114	0.807	37.9	3.458	0.104	090308	
19291709-2034504	0.923	20.7	1.304	0.146	0.675	20.4	1.134	0.139	100516	
19293586+0433277	1.309	48.7	3.190	0.090	0.638	48.6	1.866	0.108	100506	
19304765+1059508	0.371	-2.2	1.060	0.060	0.226	-2.2	0.277	0.059	090308	
19323315+1102306	0.406	11.9	1.027	0.094	0.641	12.2	2.054	0.093	090308	
19324583+0234383	0.640	13.9	1.282	0.089	0.414	16.2	1.481	0.091	100512	
19344122+1455539	0.766	-29.9	1.952	0.082	0.876	-29.5	2.284	0.085	090308	
19381020+3823403	0.473	9.2	1.390	0.085	0.391	9.5	1.484	0.090	100511	
19385776+2830467	0.691	-97.4	2.655	0.078	2.407	-98.2	4.860	0.108	050523	
19390785+1451271	0.841	53.8	2.372	0.103	0.448	52.8	1.246	0.101	100516	
19420841+4722567	0.494	-9.5	1.164	0.081	0.392	-6.8	1.054	0.083	100428	
19421995+7102137	0.335	-9.7	1.052	0.067	0.407	-9.1	0.937	0.082	100506	
19440213+2746055	1.432	7.1	1.848	0.117	1.101	7.0	1.105	0.109	100516	
19454354+4527431	0.898	2.7	1.519	0.146	1.710	3.0	2.996	0.148	100428	
19462548+3628454	0.390	-27.9	1.509	0.068	0.345	-27.3	0.820	0.078	101220	
19575512+3146002	0.927	42.4	4.696	0.078	1.489	42.8	4.300	0.068	110112	
19590895+1733197	1.468	31.7	6.732	0.150	1.445	31.7	4.570	0.141	100512	
19592317+0006104	0.923	-5.3	4.157	0.115	1.033	-3.4	5.024	0.115	051222	
19595132+3232098	1.067	4.7	6.390	0.112	1.147	8.8	5.390	0.117	100511	
20021291+3057556	0.406	30.7	0.785	0.085	0.283	32.9	0.860	0.080	100512	
20030816+2517265 ⁴	0.603	24.9	2.611	0.085	0.543	26.2	2.918	0.085	090307	
20054924+4721527	0.568	-70.0	1.626	0.097	0.386	-67.3	1.969	0.103	100428	
20074663+3117241	0.709	43.9	2.105	0.098	1.104	43.9	2.102	0.107	100511	
20115624+5429092	0.503	-59.1	1.275	0.086	0.532	-59.2	1.375	0.084	090308	
20125796+3214563	0.367	51.6	2.552	0.061	0.292	55.3	0.740	0.070	100316	
20140191+5854355	0.264	-60.7	0.745	0.054	0.274	-61.4	0.900	0.061	101220	
20192988+6305364	0.673	-19.4	2.774	0.089	0.350	-19.5	1.318	0.094	100428	
20195560+8816277	0.622	-89.1	2.372	0.061	0.491	-88.7	0.990	0.064	100321	
20214815+3603251	0.827	10.3	2.913	0.113	0.749	9.7	1.552	0.111	100516	
20224015+5200579	1.974	-5.1	6.929	0.135	1.626	-5.1	5.436	0.124	100428	
20243989+4810094	0.209	-8.5	1.161	0.059	0.282	-8.6	1.049	0.053	100517	
20293249+6702115	0.246	-25.5	0.596	0.066	0.812	-29.4	1.181	0.067	100516	
20305733+2938363	2.260	39.3	5.864	0.103	1.971	39.1	5.022	0.099	100516	
20310052+3304430	0.906	-0.8	3.192	0.145	0.783	3.2	2.767	0.117	100511	
20342260+1544440	0.415	-20.2	1.365	0.107	0.385	-18.7	0.713	0.098	100511	
20370015+3354089	1.306	4.9	3.214	0.132	1.059	9.6	3.727	0.130	100512	
20412744+5113298	0.973	-12.8	2.956	0.104	1.072	-12.7	2.789	0.105	100518	
20414535+3353226	0.000	0.0	0.000	0.061	0.186	25.1	0.553	0.060	100518	
20421889-0815307	0.618	-51.4	0.791	0.133	1.585	-51.4	2.080	0.129	100516	
20422178+2728476	0.587	14.7	2.467	0.080	0.561	14.3	1.040	0.056	101220	
20434100+3809561	1.168	15.6	5.271	0.090	0.614	15.2	1.565	0.091	100511	
20442513-0450007	5.619	-22.2	22.549	0.124	4.609	-22.3	14.189	0.136	100525	
20452605+3745328	0.284	-13.0	0.666	0.078	0.251	-12.9	0.355	0.079	100518	
20465378+0551292	0.314	63.0	0.539	0.050	0.345	63.4	0.588	0.048	100511	
20474604+1920068	5.368	-15.4	12.368	0.119	6.949	-15.4	12.468	0.119	100511	
20492117+5031512	1.257	-29.1	6.745	0.096	1.065	-24.6	5.618	0.126	100506	
20523214+2710275	0.880	-21.7	2.640	0.099	1.231	-22.8	3.090	0.113	101220	
20525979+2322159	0.468	11.0	1.820	0.090	1.783	7.6	7.680	0.106	101220	
20534219-0138066	1.419	-18.6	5.486	0.129	1.770	-16.3	5.675	0.141	100511	
20550998+6701580	0.545	-37.7	2.240	0.094	0.691	-37.5	1.016	0.095	100518	
20561005+8303252 ⁵	3.650	31.8	17.102	0.092	2.570	32.4	13.273	0.102	100321	
20592292+5853328	3.242	-30.1	7.345	0.123	3.575	-30.1	8.554	0.121	100405	
21013447+5129534	0.255	-34.8	0.662	0.062	0.216	-36.5	0.765	0.057	100517	

Table 1. (Continued.)

2MASS name (J—)	SiO $J = 1-0$ $v = 1$ maser line				SiO $J = 1-0$ $v = 2$ maser line				rms (K)	obs. date (yyymmdd.d)
	T_a (K)	V_{lsr} (km s $^{-1}$)	L.F. (K km s $^{-1}$)	rms (K)	T_a (K)	V_{lsr} (km s $^{-1}$)	L.F. (K km s $^{-1}$)	rms (K)		
21055966+2924220	0.330	-35.9	0.764	0.097	0.328	-32.7	0.891	0.097	100511	
21084764+0110146	4.628	21.7	10.421	0.136	3.732	21.9	8.393	0.136	100511	
21142956+0748337	2.702	28.6	5.655	0.128	2.081	28.7	4.453	0.126	100511	
21192721+6126125	0.369	-8.0	1.077	0.080	0.528	-8.0	0.965	0.078	100518	
21194864+5016575	0.495	-65.2	1.332	0.084	0.885	-64.8	2.081	0.075	090308	
21222904+2159543	0.181	2.0	0.261	0.044	0.246	1.9	0.420	0.049	101220	
21254399+4532327	0.497	5.3	1.242	0.095	0.436	8.1	0.728	0.102	100405	
21305815+4629283	0.507	49.9	1.072	0.098	0.704	50.0	0.690	0.113	101220	
21404842+4949446	0.523	-59.7	1.536	0.093	0.352	-59.9	0.494	0.088	100405	
21485148+3956466	2.284	0.9	4.436	0.105	2.763	1.7	5.956	0.114	100321	
21492590+4322247	0.498	-19.0	1.940	0.078	0.806	-18.5	2.482	0.083	100405	
21545410+5128444	2.350	-21.8	9.574	0.085	1.730	-19.7	9.133	0.089	100321	
21550333+4945406	0.310	-38.2	0.565	0.068	0.498	-39.3	1.057	0.065	090308	
21563802+3620341	1.288	-19.1	4.154	0.104	0.670	-19.5	1.734	0.105	100516	
22071622+1153158 [†] ⁶	60.161	23.3	134.019	0.124	41.517	23.3	77.849	0.106	090309	
22162185+4744237	2.034	-64.7	6.842	0.106	0.970	-64.2	4.800	0.110	100412	
22325976+6654394	—	—	—	0.053	0.240	-9.8	0.791	0.056	100321	
22361244+7204404	0.576	17.0	2.810	0.076	0.419	16.7	1.100	0.077	100321	
22482256+4911596	0.912	-56.2	5.952	0.052	0.342	-54.1	2.643	0.055	100412	
22490803+2452563	2.088	-49.9	11.899	0.119	1.467	-49.5	5.691	0.112	100512	
22502517+6015411	1.231	-61.4	4.259	0.097	1.771	-63.0	5.192	0.106	100411	
22504945+6415047	3.431	34.4	22.110	0.162	3.257	40.4	14.949	0.172	100405	
22521809+3413364	0.411	-12.5	1.036	0.066	0.253	-12.9	0.526	0.067	100512	
22593446+4250302	1.297	-1.0	4.129	0.122	1.043	-0.7	2.165	0.116	100405	
23041981+6745358	0.917	-50.4	4.707	0.105	0.755	-54.8	3.798	0.106	100405	
23043019+6445476	1.318	-20.1	6.410	0.113	1.913	-22.6	5.571	0.121	100227	
23055847+6014593	0.603	-21.7	1.875	0.091	0.575	-22.5	1.095	0.112	100227	
23101295+4011462	0.486	9.2	0.940	0.097	0.499	9.4	1.215	0.110	100405	
23143356+5715208	—	—	—	0.050	0.209	-15.8	0.377	0.053	100412	
23203758+3937140	9.307	-1.9	23.264	0.123	9.943	-2.1	20.176	0.124	100405	
23373973+5850458	5.443	-89.9	16.920	0.106	2.911	-89.9	9.987	0.106	100321	
23430657+3528452	0.583	-25.7	1.659	0.102	0.581	-25.5	2.158	0.104	100405	
23520899+6634495	2.159	-59.6	5.212	0.128	1.272	-59.5	3.024	0.145	100227	

[†] indicates additional detections in the ^{28}SiO $v = 0$ or 3, or ^{29}SiO $v = 0$ $J = 1-0$ line. see table 3.

¹ previous detection of the SiO $J = 2-1$ $v = 1$ line (Haikala et al. 1994).

² previous detection of the SiO $J = 1-0$ $v = 1$ and 2 line by Deguchi et al. (2010), ³ Deguchi et al. (2004),

⁴ Jiang et al. (1999), ⁵ Cho et al. (1996)⁶, Zuckerman (1979), ⁷Hall et al. (1990), ⁸ Kim et al. (2010)

Table 2. Negative results for the SiO $J = 1-0$ $v = 1$ and 2 lines.

2MASS name (J—)	$v = 1$		$v = 2$	obs. date (yymmdd.d)
	rms (K)	rms (K)		
00074306+7414113	0.070	0.077	100225	
00360130+5754427	0.092	0.087	090309	
00372236+5342117	0.081	0.098	100225	
00500597+6445351	0.077	0.090	100225	
01003486+5536221	0.092	0.097	101113	
01103043+4506115	0.092	0.097	100412	
02195542+5328072	0.086	0.089	100412	
02302753+6231456	0.108	0.102	090309	
02323488+6825324	0.098	0.103	100412	
02332877+4539162	0.087	0.088	080426	
02434850+3615022	0.183	0.185	080426	
02565576+5438358	0.121	0.124	080426	
03304049+6724078	0.063	0.075	100222	
03394128+3616044	0.058	0.064	100222	
03430321+6835275	0.110	0.114	100412	
03480562+5934563	0.071	0.075	100222	
03511623+3302069	0.106	0.114	100412	
04051774+4121023	0.057	0.059	100222	
04110273+4640253	0.056	0.058	100222	
04132963–1023138	0.081	0.076	080413	
04190835+5738225	0.055	0.055	100222	
04212725+0129134	0.040	0.040	101208	
04215740+2826355	0.108	0.103	100302	
04233661+3838036	0.142	0.121	090506	
04240873+6813180	0.057	0.057	100222	
04252721+1633233	0.145	0.149	090506	
04324806+2239523	0.093	0.115	100227	
04363710+3704451	0.135	0.122	090506	
04462516+5428507	0.070	0.073	100222	
04470673+2610455	0.095	0.091	100405	
04591899+1545118	0.086	0.083	100405	
05104212+3357144	0.074	0.077	090323	
05194379+2610352	0.065	0.066	100405	
05221592+0837391	0.102	0.100	090323	
05285405–0606063	0.116	0.143	100227	
05312805+1209102	0.049	0.043	101208	
05415139–0854565	0.147	0.146	100412	
05490369+1911005	0.080	0.080	090323	
05534254–1024007	0.070	0.065	101209	
06101597+0256268	0.087	0.083	100302	
06123120–2710145	0.068	0.067	101209	
06140002+2742122	0.093	0.088	090323	
06290218–0039203	0.079	0.083	100302	
06320728+0143006	0.142	0.141	090505	
06341217+1416346	0.151	0.153	100412	
06411508–2216436	0.070	0.059	101209	
06505251–0004235	0.048	0.043	080405	
07101638–1615491	0.089	0.098	100225	
07205859–1022441	0.161	0.165	080413	
07252277–0335508	0.087	0.075	101207	
07304746–0946366	0.098	0.092	080413	
07485921–1102277	0.085	0.081	090321	
07521749–0329044	0.087	0.081	090321	
07524790–1026439	0.100	0.100	090321	
08034242–3126459	0.111	0.119	100225	
09510854–2953451	0.091	0.074	080411	
10484663+0839579	0.095	0.074	080413	
11293071–1856182	0.060	0.067	100225	
17313400–0818559	0.088	0.000	100315	
17484719+0159472	0.101	0.098	100512	
17590076–1133231	0.078	0.073	100315	
18141650+1409344	0.073	0.063	080427	
18144939+0512556	0.065	0.070	080427	
18162366–0259033	0.111	0.107	100512	
18251801–1151109	0.088	0.088	100315	
18330727–0530138	0.079	0.076	100315	

Table 2. (Continued.)

2MASS name (J—)	$v = 1$		$v = 2$	obs. date (yyymmdd.d)
	rms (K)	rms (K)		
18373020+0148410	0.069	0.073		100316
18380236+0213546	0.089	0.091		100511
18390434+0141173	0.075	0.079		100511
18391616−0340489	0.093	0.093		100511
18494283+0141017	0.077	0.077		090307
18513199+1757581	0.087	0.080		100512
18523589−0312163	0.114	0.113		100511
18535746+0136407	0.109	0.112		100511
18545593−0121217	0.108	0.104		100511
18590914+1023398	0.075	0.071		090307
19031282+3358117	0.081	0.081		110112
19060808+0441110	0.087	0.082		090307
19080470+0248571	0.084	0.073		090307
19143038+1050456	0.060	0.066		101220
19194716+2248220	0.080	0.078		090307
19253109+4552428	0.080	0.102		100506
19272030+1139227	0.051	0.052		090308
19325060+2117217	0.082	0.081		090308
19354575+1650318	0.083	0.079		090308
19365303+2519359	0.137	0.134		100512
19382455+2123132	0.089	0.080		100516
19414554+4212326	0.089	0.091		100428
19430452+2331452	0.113	0.108		100516
19473259+0834449	0.101	0.101		100516
19483842+2759358	0.082	0.077		100511
19514353+5341314	0.064	0.073		101220
19554461+2604497	0.080	0.087		100512
19570502+3949363	0.097	0.105		100511
19582591+2520238	0.068	0.067		100512
20011298+1929375	0.063	0.072		101220
20051813+3822231	0.080	0.081		090307
20054586+3758597	0.088	0.083		090307
20055019+1914390	0.061	0.063		101220
20091038+2157020	0.061	0.077		101220
20103451+3327260	0.083	0.084		100511
20135576+3923489	0.092	0.095		100428
20142861+5944210	0.096	0.097		100428
20175937+4317424	0.079	0.082		101220
20184764+2846120	0.078	0.074		090308
20204822+4520446	0.080	0.085		100518
20211825+3812440	0.108	0.099		100516
20222536+6944465	0.097	0.096		100428
20254959+3126054	0.112	0.108		100516
20255026+3701465	0.115	0.103		100516
20264303+4056268	0.112	0.107		100516
20361159+3507454	0.087	0.089		100512
20374385+4334417	0.098	0.099		090307
20443146+3229319	0.056	0.052		100511
20474862+5402373	0.087	0.076		100517
20500496+3729598	0.097	0.098		100511
20545041+4115401	0.057	0.066		101220
20575361+4245544	0.079	0.084		090307
21010281+3932493	0.081	0.074		090308
21010620+5007568	0.091	0.093		100428
21045803+2723558	0.073	0.085		101220
21130526+5025299	0.109	0.112		100405
21134983+6151234	0.070	0.084		101220
21174247+4603477	0.094	0.096		100405
21182190+4957472	0.113	0.113		100405
21231933+2328482	0.070	0.073		100516
21232465+2314599	0.064	0.071		101220
21302607+5009190	0.074	0.083		101220
21354271+6839071	0.100	0.102		100405
21461997+4806502	0.091	0.087		100428
21561897+5848227	0.084	0.092		100411

Table 2. (Continued.)

2MASS name (J—)	<i>v</i> = 1		<i>v</i> = 2		obs. date (yymmdd.d)
	rms (K)	rms (K)	rms (K)	obs. date (yymmdd.d)	
21575765+6310007	0.074	0.076	0.076	090308	
21582612+5324124	0.092	0.100	0.100	100411	
22062959+5929281	0.083	0.086	0.086	100321	
22063776+5941202	0.081	0.086	0.086	100321	
22182648+6705527	0.076	0.076	0.076	100321	
22213319+7340270	0.105	0.099	0.099	100428	
22373599+6116091	0.076	0.076	0.076	100321	
22403720+6630334	0.077	0.760	0.760	100411	
22470407+5845143	0.079	0.080	0.080	100411	
22491046+5918129	0.119	0.114	0.114	100405	
23052739+5707463	0.072	0.078	0.078	100411	
23132411–1519163	0.166	0.184	0.184	080426	
23162591+3843473	0.085	0.084	0.084	100405	
23181054+6552436	0.120	0.247	0.247	101213	
23203705+6732137	0.098	0.113	0.113	100412	
23395874+6320547	0.088	0.070	0.070	090309	
23402236+7026294	0.092	0.103	0.103	100412	
23422673+6337387	0.147	0.134	0.134	090309	
23430569+6002467	0.104	0.109	0.109	100412	

Table 3. Observational results for additional SiO lines

2MASS name (J—)	transition	<i>T</i> _a (K)	<i>V</i> _{lsr} (km s ⁻¹)	L.F. (K km s ⁻¹)	rms (K)	obs. date (yymmdd.d)
00504329+4630307	²⁹ SiO <i>v</i> = 0 <i>J</i> = 1–0	0.382	−34.5	0.739	0.086	100222
01070453+4924467	²⁸ SiO <i>v</i> = 3 <i>J</i> = 1–0	0.316	−57.7	0.445	0.081	100222
05572394+4822417	²⁹ SiO <i>v</i> = 0 <i>J</i> = 1–0	0.521	2.2	0.835	0.084	100222
05572394+4822417	²⁸ SiO <i>v</i> = 3 <i>J</i> = 1–0	1.629	2.8	4.406	0.105	100222
05581447+5002407	²⁹ SiO <i>v</i> = 0 <i>J</i> = 1–0	0.305	−43.2	1.012	0.070	100222
14045992–3529505	²⁸ SiO <i>v</i> = 0 <i>J</i> = 1–0	0.438	−1.3	2.274	0.108	100223
18272417–0100456	²⁹ SiO <i>v</i> = 0 <i>J</i> = 1–0	0.728	−7.3	2.443	0.153	100315
18541840–0648564	²⁹ SiO <i>v</i> = 0 <i>J</i> = 1–0	0.595	−20.8	1.066	0.116	100511
19261909+1640323	²⁹ SiO <i>v</i> = 0 <i>J</i> = 1–0	0.374	9.6	0.723	0.087	090308
22071622+1153158	²⁹ SiO <i>v</i> = 0 <i>J</i> = 1–0	0.836	23.3	0.542	0.095	090309
22071622+1153158	²⁸ SiO <i>v</i> = 3 <i>J</i> = 1–0	4.141	23.2	6.127	0.125	090309
22071622+1153158	²⁸ SiO <i>v</i> = 0 <i>J</i> = 1–0	0.334	19.1	0.505	0.104	090309

Table 4. Infrared properties of the observed objects

2MASS name (J—)	Period (d)	<i>K</i> mag.	<i>H</i> — <i>K</i>	<i>F</i> ₁₂ (Jy)	<i>C</i> ₁₂	<i>V</i> _{lsr} (<i>SiO</i>) (km s ⁻¹)	IRAS/MSX name	comment
00074306+7414113	476	4.64	1.12	7.4	-0.492		00050+7357	
00100914+5452343	730	3.04	0.70	15.2	-0.377	-35.2	00075+5435	
00163648+6601104	330	4.24	0.67	2.5	-0.286	-60.7	00138+6544	
00202547+6947567	425	2.86	0.86	18.6	-0.406	-49.5	00176+6931	
00251001+7008516	454	2.33	0.73	25.0	-0.330	-42.3	00222+6952	
00360130+5754427	301	4.81	0.44	2.1	-0.450		00331+5738	
00365942+6308016	730	3.07	0.80	50.4	-0.415	-57.2	00340+6251	H ₂ O ^{2,3}
00372236+5342117	176 [†]	2.86	0.61	8.2	-0.439		00345+5325	
00382283+8021250	332	2.46	0.65	16.5	-0.410	2.9	00347+8004	
00452805+7550219	599	4.47	0.87	15.1	-0.103	-82.8	00420+7533	
00480999+5334010	298	2.56	0.62	11.7	-0.421	-42.0	00453+5317	
00500597+6445351	302 [†]	6.99	0.93	4.6	0.028		00470+6429	
00504329+4630307	349	3.97	0.81	36.7	-0.114	-34.2	00479+4614	
00532514+6501559	727	3.77	0.73	14.4	-0.316	-17.4	00503+6445	
01003486+5536221	398	5.11	0.67	4.6	-0.332		00576+5520	
01052742+6558594	341	2.72	0.64	20.4	-0.396	-63.3	01022+6542	
01070453+4924467	405	3.18	0.65	19.2	-0.275	-58.5	01041+4908	
01103043+4506115	362	3.81	0.80	6.3	-0.391		01076+4450	
01215470+6120551	288	3.33	0.76	9.3	-0.377	-31.0	01186+6105	
01564706+3401107	287	3.32	0.60	7.1	-0.331	-121.4	01538+3346	
02055459+4043267	413	2.60	0.63	26.8	-0.345	-14.9	02028+4029	
02195542+5328072	398 [†]	5.69	1.23	4.0	-0.370		02165+5314	
02201452+7845362	403	2.55	0.76	34.1	-0.354	-27.9	02145+7831	H ₂ O ¹
02302753+6231456	440	3.60	0.55	6.0	-0.328		02266+6218	
02304255+6635004	467	5.54	0.94	8.1	-0.262	-56.0	02265+6621	
02323488+6825324	405	4.09	0.69	7.1	-0.353		02283+6812	
02332877+4539162	200	-0.02	0.36	134.0	-0.219		02302+4525	
02431547+8108095	498	2.39	0.80	19.7	-0.316	-57.2	02361+8055	
02434850+3615022	358 [†]	2.79	0.56	61.2	-0.098		02407+3602	
02444549+1219029	519	2.60	0.61	15.5	-0.222	20.4	02420+1206	OH ⁴ , H ₂ O ⁵
02522580+3641298	403	2.78	0.63	19.0	-0.222	-61.0	02493+3629	
02561803+4553132	274	4.51	0.87	29.9	-0.261	-49.7	02529+4541	
02565576+5438358	150 [†]	0.67	0.31	68.5	-0.337		02532+5426	
02572747+1118057	324	3.95	0.74	31.5	-0.037	15.4	02547+1106	OH ⁴
03043767+5649144	223	4.35	0.73	10.7	-0.302	-12.4	03008+5637	
03194960+6120515	348	4.22	0.78	6.2	-0.322	-100.3	03157+6110	
03304049+6724078	491	4.71	1.46	10.5	-0.427		03259+6713	
03323218+7427045	336	3.72	0.67	8.5	-0.400	-51.7	03268+7416	
03394128+3616044	730	4.82	0.86	14.6	-0.245		03364+3606	
03430321+6835275	188 [†]	3.13	0.67	6.3	-0.262		03381+6825	
03480562+5934563	226 [†]	2.31	0.63	16.9	-0.231		03439+5925	
03483231+3216437	368	4.16	0.62	8.6	-0.119	-21.0	03453+3207	
03511623+3302069	730	3.34	0.83	8.7	-0.340		03480+3253	
03542359+1601019	244	4.40	0.65	3.3	-0.305	45.5	03515+1552	
04051774+4121023	197 [†]	4.09	0.67	3.9	-0.192		04018+4112	
04110273+4640253	185 [†]	4.97	0.63	3.3	-0.154		04074+4632	
04132963-1023138	559 [†]	1.36	0.28	28.2	-0.390		04111-1030	
04153489+3349461	436	2.57	0.71	31.4	-0.373	-72.9	04123+3342	
04190835+5738225	139 [†]	3.16	0.84	5.3	-0.336		04149+5731	
04212541+2015592	312	3.15	0.81	16.0	-0.486	45.2	04184+2008	
04212725+0129134	359 [†]	6.42	1.49	3.4	-0.452		04188+0122	
04215740+2826355	82 [†]	5.39	0.73	17.5	0.174		04188+2819	
04232410+0634322	730	4.02	0.54	7.7	-0.268	-22.6	04207+0627	
04233661+3838036	278	3.80	0.51	6.4	-0.387		04202+3831	
04240873+6813180	372	3.13	0.61	5.6	-0.370		04190+6806	
04252721+1633233	258	3.20	0.59	5.9	-0.480		04225+1626	
04324806+2239523	323 [†]	2.75	0.76	13.4	-0.309		04298+2233	
04341277+4715357	363	2.83	0.65	15.5	-0.375	2.4	04305+4709	
04355719+2830524	418 [†]	1.57	0.68	54.6	-0.389	-5.8	04328+2824	
04363710+3704451	131 [†]	2.74	0.59	8.7	-0.335		04332+3658	
04402801+3016500	678	2.64	0.80	23.1	-0.451	-100.1	04372+3011	
04462516+5428507	331 [†]	4.60	1.27	6.1	-0.496		04423+5423	
04470673+2610455	236	4.78	0.71	22.5	-0.097		04440+2605	
04505728+0308323	672	4.46	0.70	5.6	-0.262	-13.2	04483+0303	
04553028+0304281	240	4.62	0.60	3.6	-0.362	47.0	04528+0259	
04591899+1545118	405	5.61	1.27	4.5	-0.457		04564+1540	

Table 4. (Continued.)

2MASS name (J—)	Period (d)	<i>K</i> mag.	<i>H</i> − <i>K</i>	<i>F</i> ₁₂ (Jy)	<i>C</i> ₁₂	<i>V</i> _{lsr} (<i>SiO</i>) (km s ^{−1})	IRAS/MSX name	comment
05001777+6046152	501	3.56	0.79	10.7	−0.210	−52.2	04557+6041	
05104212+3357144	379	4.33	0.58	2.9	−0.410		05073+3353	
05194379+2610352	346	3.91	0.66	4.6	−0.479		05166+2607	
05221592+0837391	482	5.79	1.50	9.1	−0.520		05195+0834	
05285405−0606063	271	5.58	0.71	6.7	−0.328		05264−0608	
05312805+1209102	69†	7.34	0.97	3.8	0.031		05286+1207	
05381725+4700121	509	3.34	0.81	9.3	−0.415	−13.9	05345+4658	
05413366−0407549	238	2.25	0.61	26.2	−0.385	44.4	05390−0409	
05415139−0854565	150†	2.91	0.63	8.4	−0.344		05394−0856	
05435348+0310111	317	2.96	0.60	10.4	−0.332	60.3	05412+0308	
05490369+1911005	179†	5.17	0.54	1.3	−0.264		05460+1910	
05490636−3220002	329	2.78	0.60	19.1	−0.307	23.5	05472−3220	
05505493+0018131	716	3.09	0.68	11.1	−0.381	22.3	05483+0017	
05534254−1024006	361‡	5.96	1.68	17.5	0.167		05513−1024	
05572394+4822417	730	2.02	0.74	40.9	−0.197	2.9	05535+4822	
05581447+5002407	730	3.21	1.04	31.4	−0.164	−43.8	05543+5002	
06015218+2149051	426	3.56	0.67	8.4	−0.421	21.0	05588+2149	
06101597+0256268	86†	4.12	0.66	4.2	−0.223		06076+0257	
06123120−2710144	399	4.07	1.16	11.8	−0.497		06105−2709	
06140002+2742122	730	7.58	1.45	7.9	−0.144		06108+2743	
06290218−0039203	185†	3.95	0.60	3.4	−0.232		06264−0037	
06320728+0143006	345†	3.19	0.50	6.1	−0.334		06295+0145	
06340951−1017085	287	4.25	0.65	3.5	−0.437	34.4	06317−1014	
06341217+1416346	386†	4.11	1.17	7.4	−0.200		06313+1418	
06411508−2216435	403‡	2.56	0.88	23.6	−0.352		06391−2213	
06450560+0902184	537	2.23	0.64	52.5	−0.335	33.4	06423+0905	OH ⁶
06505251−0004235	305‡	2.33	0.42	19.1	−0.160		06483−0000	
06570903+4735220	352	2.80	0.67	20.4	−0.376	−9.0	06534+4739	
06574519+0318093	204†	2.01	0.64	36.6	−0.368	−9.5	06551+0322	
07072185+2817559	355	2.91	0.84	20.6	−0.310	−48.7	07042+2822	
07073432+2413190	459	4.09	0.61	14.8	−0.172	38.4	07045+2418	
07100587+6556246	459	3.29	0.93	52.9	−0.220	10.4	07051+6601	
07101638−1615491	157‡	1.82	0.51	29.9	−0.308		07080−1610	
07125372+1739161	279	2.80	0.54	16.9	−0.398	−11.5	07099+1744	
07205859−1022441	68‡	1.86	0.44	23.8	−0.280		07186−1017	
07252276−0335507	1131‡	5.71	0.32	0.3	−0.129		R07228−0329‡	
07304746−0946366	91‡	4.04	0.23	124.0	−0.147		07284−0940	
07314247+4733226	365	4.01	0.63	3.7	−0.390	−37.8	07280+4739	
07485921−1102277	730	3.39	0.51	8.8	−0.374		07466−1054	
07521749−0329044	124†	4.23	0.55	5.1	−0.149		07497−0321	
07524790−1026439	375	4.29	0.57	5.2	−0.393		07504−1018	
07553633−3936228	379	1.40	0.53	52.5	−0.388	40.8	07538−3928	
07555070+5711533	422	2.07	0.65	16.6	−0.396	36.5	07517+5719	
08034242−3126459	674‡	2.24	0.54	18.2	−0.264		08017−3118	
08093981−3810285	327	0.05	0.52	110.7	−0.404	−34.6	08078−3801	
08102916−3247207	679	4.38	0.84	40.2	−0.336	54.2	08085−3238	
08170543−3126193	364	2.33	0.68	35.0	−0.360	22.0	08150−3117	
08254033−2210342	730	4.39	0.62	4.8	−0.262	92.5	08234−2200	
08355329−1911284	469	5.11	0.77	13.1	−0.343	54.3	08336−1901	
08400691−0813472	730	3.84	0.79	12.8	−0.197	23.2	08376−0803	
08414614+0211202	310	2.74	0.68	56.2	−0.136	−32.3	08391+0222	
08520560−3305439	256	2.64	0.60	25.1	−0.116	57.9	08500−3254	
09243332−3043520	458	3.79	0.77	35.3	−0.280	48.7	09224−3030	
09422273+7751074	350	2.75	0.67	17.0	−0.400	21.1	09368+7804	
09510854−2953451	453‡	1.19	0.37	40.3	−0.325		MSX ^{G7}	
09572218−0232555	311	3.98	0.70	5.1	−0.419	−2.4	09548−0218	
10484663+0839579	127‡	1.71	0.40	26.3	−0.200		MSX ^{G8}	
11293071−1856182	263†	4.39	0.62	3.3	−0.300		11269−1839	
11353071+3452042	915‡	−0.22	0.36	145.4	−0.276	2.5	MSX ^{G9}	
12002079−1011049	285	3.58	0.53	15.1	−0.376	−4.3	11577−0954	
12505315−2950431	290	2.76	0.51	11.2	−0.360	−39.0	12481−2934	
13512546−3656376	328	2.73	0.57	16.0	−0.320	3.6	13484−3641	
13564515−2532429	219	4.35	0.62	9.5	−0.384	21.8	13539−2518	
13574319−3104110	274	2.10	0.54	46.6	−0.440	−1.8	13548−3049	
14045992−3529505	377	1.76	0.67	239.9	−0.408	3.9	14020−3515	H ₂ O ¹⁰
16385186+1403583	271	1.67	0.51	24.6	−0.450	−28.3	16365+1409	

Table 4. (Continued.)

2MASS name (J—)	Period (d)	<i>K</i> mag.	<i>H</i> – <i>K</i>	<i>F</i> ₁₂ (Jy)	<i>C</i> ₁₂	<i>V</i> _{lsr} (<i>SiO</i>) (km s ^{–1})	IRAS/MSX name	comment
16510590+1020515	303	3.02	0.65	10.5	–0.353	19.2	16487+1025	
16523612–0527277	275	4.44	0.61	3.2	–0.350	9.6	16499–0522	
16582342–2054105	353	3.25	0.64	13.6	–0.372	76.0	16554–2049	
16584672–1243469	286 [†]	6.19	0.80	3.9	–0.249	–62.7	16559–1239	
16594972+5219044	278	2.78	0.60	9.0	–0.383	–32.7	16586+5223	
17040522+7147470	336	3.69	0.65	8.4	–0.421	–54.4	17048+7151	
17192766–1015403	293	5.12	0.66	3.4	–0.203	73.5	17167–1012	
17253651+0111059	730	3.80	0.54	25.3	–0.067	–19.6	17230+0113	
17272100–0613166	397	3.35	0.60	10.3	–0.422	75.6	17246–0610	
17280830+0502185	369	3.29	0.68	18.3	–0.081	25.2	17256+0504	OH ⁷ , H ₂ O ⁸
17313400–0818559	84 [†]	3.90	0.60	3.1	–0.346		17288–0816	
17381195–1241572	350	4.77	0.77	8.1	–0.286	28.6	17353–1240	
17392120–1312145	343	4.41	0.86	9.1	–0.232	0.2	17365–1310	
17424879–0146555	615	4.37	0.66	10.0	–0.246	22.2	17402–0145	
17444713+5437173	361	3.08	0.68	12.9	–0.339	–41.0	17437+5438	
17445378+2129466	329	2.88	0.65	10.1	–0.406	–32.8	17427+2130	
17484719+0159472	361	5.19	0.63	4.6	–0.275		17462+0200	
17590076–1133231	405	3.86	0.78	8.3	–0.410		17562–1133	
18032344–0218030	594	4.50	0.62	3.2	–0.386	52.8	18007–0218	
18050458+0246114	445	3.90	0.61	6.8	–0.252	59.2	18025+0245	
18074103–0518196	287	4.76	1.15	35.7	–0.064	–27.5	18050–0518	
18141650+1409344	105 [‡]	4.38	0.53	14.6	–0.147		18120+1408	
18144939+0512556	387 [‡]	6.73	0.67	10.7	0.012		18123+0511	
18154122–0331121	389	3.64	0.76	8.1	–0.368	–37.2	18130–0332	
18162366–0259033	371	4.34	0.91	9.6	–0.357		18137–0300	
18223780+0637444	503	3.33	0.67	15.5	–0.304	67.1	18202+0636	
18230711–0146024	476	4.48	0.65	16.3	–0.163	74.6	18205–0147	
18230994–0636023	392	3.16	0.63	12.1	–0.381	3.2	18204–0637	
18234044–0421328	306	4.82	1.12	9.2	–0.289	11.8	18210–0423	
18250094–0650575	271	3.56	0.60	9.7	–0.423	96.8	18223–0652	
18251801–1151109	281 [†]	3.12	0.97	43.5	–0.269		18225–1152	
18260088+5055498	373	3.50	0.70	7.8	–0.385	2.7	18248+5053	
18272417–0100456	426	3.33	0.90	21.3	–0.019	–7.3	18248–0102	
18274054+4918331	358	2.94	0.64	14.4	–0.362	13.9	18264+4916	
18285243+0150161	437	3.99	0.88	5.7	–0.316	57.5	18263+0148	
18330727–0530138	103 [†]	4.43	0.63	6.0	–0.174		18304–0532	
18335184+0342484	387	3.29	0.89	11.9	–0.354	40.1	18313+0340	
18361528+0126242	354	3.29	1.10	11.4	–0.343	40.6	18337+0123	
18371700+0615306	730	4.47	0.73	8.1	–0.293	49.5	18348+0612	
18373020+0148410	231 [†]	3.88	0.76	5.5	–0.152		18349+0146	
18373693+1309559	476	3.06	0.72	8.8	–0.382	67.3	18353+1307	
18380236+0213546	233 [†]	3.58	0.82	4.0	–0.221		18355+0211	
18390434+0141173	423	2.77	0.69	11.5	–0.406		18365+0138	
18391616–0340489	339	3.99	1.02	24.6	–0.251		18366–0343	
18391722–0320102	548	3.97	1.08	39.5	0.003	5.0	18366–0322	
18395233–0423328	730	3.91	0.65	7.0	–0.180	65.4	18372–0426	
18401649+0004131	213	3.35	0.91	7.9	–0.380	–29.0	18377+0001	
18420997+1038548	730	3.70	0.74	11.7	–0.227	68.4	18398+1035	
18422141+0208504	709	3.15	0.76	11.8	–0.339	50.1	18398+0205	
18424774+1548565	182 [†]	3.54	0.68	9.1	–0.373	–10.0	18405+1545	
18440224–0638441	349	3.81	0.64	5.3	–0.266	62.5	18413–0641	
18451727+0056300	323	4.51	0.78	3.3	–0.291	64.2	18427+0053	
18473513–0651009	379	4.59	0.68	11.2	–0.241	–24.9	18448–0654	
18482850–0540524	437	3.71	0.60	7.3	–0.369	51.8	18458–0544	
18494283+0141017	488	4.04	1.01	6.5	–0.374		18471+0137	
18513199+1757581	355	4.91	0.60	7.5	–0.354		18493+1754	
18523589–0312163	276 [†]	2.26	0.68	17.3	–0.306		18499–0316	
18533423+0048559	221	3.80	0.66	6.9	–0.319	41.5	18510+0045	
18535746+0136407	612 [†]	2.79	0.61	8.1	–0.313		18514+0132	
18541840–0648564	278	3.99	0.83	12.8	–0.260	–20.2	18516–0652	
18545593–0121217	329 [†]	3.85	0.67	23.2	–0.153		18523–0125	
18550405+0606293	360	4.61	0.86	3.4	–0.339	–5.4	18526+0602	
18551284+1041470	310	2.98	0.66	20.1	–0.329	–51.7	18528+1037	
18590914+1023398	730	3.62	0.59	9.7	–0.388		18567+1019	
19013031+0954055	730	4.48	0.67	2.1	–0.365	70.8	18591+0949	
19021502+4712597	414	3.24	0.69	10.0	–0.355	15.1	19008+4708	

Table 4. (Continued.)

2MASS name (J—)	Period (d)	<i>K</i> mag.	<i>H</i> − <i>K</i>	<i>F</i> ₁₂ (Jy)	<i>C</i> ₁₂	<i>V</i> _{lsr} (SiO) (km s ^{−1})	IRAS/MSX name	comment
19030960−0128366	374	4.61	0.81	9.9	−0.388	56.3	19005−0133	
19031282+3358117	494	4.79	0.66	6.2	−0.205		19013+3353	
19042996+0305134	587	4.01	0.73	7.0	−0.217	46.5	19020+0300	
19060808+0441110	648	5.27	0.85	1.9			MSX ^{#1}	
19080470+0248571	333	6.23	0.77	0.9			MSX ^{#2}	
19084758−0402461	730	3.02	0.63	9.5	−0.419	19.6	19061−0407	
19091839+733285	154 [†]	2.87	0.64	7.6	−0.346	−16.7	19103+7328	
19092954+0127514	256	4.84	0.68	6.9	−0.343	97.8	19069+0122	
19143038+1050456	299	3.84	0.83	7.2	−0.198		19121+1045	
19145099+0414308	423	2.23	0.54	16.3	−0.329	−40.7	19123+0409	
19145678+2204305	529	2.35	0.81	39.9	−0.241	8.4	19128+2159	
19152147+0233020	331 [†]	4.55	0.69	6.7	−0.228	56.9	19128+0227	
19154874+0945208	526	3.52	0.64	11.4	−0.275	18.1	19134+0939	
19161015+0841001	662	4.55	0.74	5.7	−0.290	34.3	19137+0835	
19163390+1822517	415	4.24	0.90	23.7	−0.226	−0.5	19143+1817	
19170076+1456093	730	4.71	0.44	4.9	−0.357	28.5	19147+1450	
19172579+4248497	393	4.05	0.68	7.1	−0.377	−21.4	19158+4243	
19194716+2248220	387	4.97	0.52	1.7	−0.457		19176+2242	
19195583+1254351	372	3.95	0.85	6.0	−0.386	−48.2	19176+1248	
19202271+0455507	354	2.94	0.55	10.9	−0.247	−2.3	19179+0450	
19221604+0506593	458	3.28	0.69	35.1	−0.255	−36.8	19198+0501	
19242261+3219082	433	2.98	0.75	20.2	−0.241	2.8	19224+3213	
19252049+0620243	402	3.75	0.54	6.3	−0.351	−46.8	19228+0614	
19253109+4552428	723 [†]	3.24	0.68	8.1	−0.300		19240+4546	
19261909+1640323	730	3.19	0.96	23.3	−0.288	17.0	19240+1634	
19265263+1644068	337	3.92	0.72	12.8	−0.270	−21.3	19246+1637	
19271451+1129045	730	2.47	0.68	28.4	−0.220	42.1	19248+1122	
19272030+1139227	383	3.48	0.46	4.6	−0.402		19249+1133	
19273109+1928141	730	5.07	1.30	25.9	−0.243	39.2	19253+1922	
19291709−2034504	417	3.89	0.68	8.7	−0.318	20.5	19263−2041	
19293586+0433277	356	4.47	0.89	17.5	−0.259	48.7	19271+0427	
19304765+1059508	335	6.00	0.53	3.3	−0.334	−2.2	19284+1053	
19323315+1102306	424	4.78	0.59	2.1	−0.316	12.0	19301+1056	
19324583+0234383	246	4.38	0.80	10.4	−0.305	15.1	19302+0228	
19325060+2117217	427	5.20	0.92	2.4	−0.360		19306+2110	
19344122+1455539	337	4.24	0.69	4.0	−0.335	−29.7	19323+1449	
19354575+1650318	311	4.10	0.67	8.6	−0.124		19334+1643	
19365303+2519359	213 [†]	2.91	0.68	9.6	−0.205		19347+2512	
19381020+3823403	323	4.34	0.62	10.1	−0.430	9.4	19364+3816	
19382455+2123132	233 [†]	2.86	0.65	7.6	−0.314		19362+2116	
19385776+2830467	288	1.06	0.22	56.0	−0.424	−97.8	19369+2823	
19390785+1451271	300	4.07	0.62	7.8	−0.334	53.3	19368+1444	
19414554+4212326	337 [†]	2.31	0.70	16.4	−0.326		19401+4205	
19420841+4722567	622	3.41	0.68	24.6	−0.168	−8.1	19406+4715	
19421995+7102137	562	4.35	0.81	16.8	−0.101	−9.4	19426+7055	
19430452+2331452	104 [†]	2.68	0.60	7.4	−0.315		19409+2324	
19440213+2746055	363	3.01	0.74	7.4	−0.302	7.1	19420+2738	
19454354+4527431	413	3.71	0.80	13.5	−0.144	2.8	19441+4520	
19462548+3628454	249	4.80	0.73	6.2	−0.246	−27.6	19445+3621	
19473259+0834449	181 [†]	4.47	0.63	7.7	−0.350		19451+0827	
19483842+2759358	730 [†]	3.68	0.61	27.8	−0.011		19466+2751	
19514353+5341314	400	4.80	0.86	5.0	−0.424		19505+5333	
19554461+2604497	115 [†]	3.35	0.69	10.8	−0.231		19536+2556	
19570502+3949363	474 ¹¹	4.76	1.04	42.8	−0.098		19553+3941	SiO ¹²
19575512+3146002	414	4.40	0.82	7.6	−0.337	42.6	19559+3137	
19582591+2520238	500 [†]	2.76	0.60	11.9	−0.206		19563+2512	
19590895+1733197	340 [†]	4.34	0.68	8.5	−0.319	31.7	19568+1725	
19592317+0006104	335	4.51	1.17	17.4	−0.039	−97.8	19568−0002	
19595132+3232098	315	3.37	0.75	18.5	−0.242	6.7	19579+3223	
20011298+1929375	182 [†]	3.33	0.75	7.5	−0.306		19589+1921	
20021291+3057556	309	4.14	0.78	8.0	−0.265	31.8	20002+3049	
20030816+2517265	398	3.53	0.77	9.1	−0.373	25.5	20010+2508	
20051813+3822231	353	6.08	0.69	1.1	−0.391		20034+3813	
20054586+3758597	381	5.10	0.51	1.1	−0.541		20039+3750	
20054924+4721527	730	5.50	1.00	10.6	−0.266	−68.7	20042+4713	
20055019+1914390	155 [‡]	2.07	0.55	10.4	−0.396		20035+1905	

Table 4. (Continued.)

2MASS name (J—)	Period (d)	K mag.	H – K	F_{12} (Jy)	C_{12}	$V_{\text{lsr}}(SiO)$ (km s $^{-1}$)	IRAS/MSX name	comment
20074663+3117241	281	3.77	1.00	14.5	-0.352	43.9	20057+3108	
20091038+2157029	123 ‡	3.13	0.85	9.0	-0.417		20069+2148	
20103451+3327260	730 †	1.91	0.86	34.1	-0.221		20086+3318	
20115624+5429092	347	4.54	0.65	3.8	-0.328	-59.2	20106+5420	
20125796+3214563	658	2.18	0.80	56.7	-0.225	53.4	20109+3205	OH 13 , H ₂ O 13
20135576+3923489	166 †	2.47	0.62	11.6	-0.253		20121+3914	
20140191+5854355	385	6.07	0.90	5.1	-0.197	-61.1	20130+5845	
20142861+5944210	173 †	2.70	0.68	21.2	-0.165		20135+5935	
20175937+4317424	142 †	3.095	0.632	6.7	-0.294		20162+4308	
20184764+2846120	308	5.69	0.69	1.4	-0.325		20167+2836	
20192988+6305364	405	4.57	0.81	11.1	-0.178	-19.5	20187+6256	
20195560+8816277	338	4.30	0.61	5.3	-0.370	-88.9	20450+8806	
20204822+4520446	289 †	3.59	0.64	5.8	-0.244		20191+4511	
20211825+3812440	184 †	2.67	0.72	8.5	-0.318		20194+3803	
20214815+3603251	257	3.78	0.69	9.0	-0.374	10.0	20198+3553	
20222536+6944465	480	3.23	1.07	17.0	-0.486		20223+6935	
20224015+5200579	730	2.98	1.03	21.3	-0.328	-5.1	20212+5151	
20243989+4810094	366	3.53	0.72	8.4	-0.342	-8.6	20231+4800	
20254959+3126054	380	3.07	0.63	7.9	-0.364		20238+3116	
20255026+3701465	179 †	3.18	0.76	7.7	-0.206		20239+3651	
20264303+4056268	122 †	3.00	0.80	10.8	-0.135		20249+4046	
20293249+6702115	423	3.45	0.70	13.5	-0.209	-27.5	20290+6652	
20305733+2938363	482	4.75	0.92	10.0	-0.167	39.2	20288+2928	
20310052+3304430	412	4.41	0.80	12.8	-0.239	1.2	20290+3254	
20342260+1544440	328	4.23	0.64	16.0	-0.221	-19.5	20320+1534	
20361159+3507454	730 †	2.68	0.74	12.2	-0.350		20342+3457	
20370015+3354089	371	4.21	0.64	14.3	-0.323	7.2	20350+3343	
20374385+4334417	389	4.58	1.03	2.7			MSX $^{\ddagger 3}$	
20412744+5113298	383	4.09	0.72	6.4	-0.320	-12.7	20399+5102	
20414535+3353226	160 †	3.33	0.64	6.3	-0.338	25.1	20397+3342	
20421889–0815307	681	3.96	0.75	11.7	-0.103	-51.4	20396–0826	
20422178+2728476	327	2.29	0.54	19.6	-0.402	14.5	20402+2718	
20434100+3809561	281	2.07	0.67	19.6	-0.410	15.4	20417+3759	H ₂ O 9
20442513–0450007	389	2.29	0.53	42.4	-0.367	-22.2	20417–0500	
20443146+3229319	408	3.20	0.71	50.2	-0.211		20425+3218	
20452605+3745328	234	3.89	0.91	7.4	-0.374	-12.9	20435+3734	
20465378+0551292	324	4.70	1.19	34.2	-0.079	63.2	20444+0540	
20474604+1920068	730	2.22	0.82	25.6	-0.170	-15.4	20454+1908	
20474862+5402373	280	4.32	0.62	7.3	-0.454		20463+5351	
20492117+5031512	536	2.94	0.85	13.1	-0.364	-26.9	20477+5020	
20500496+3729598	321 †	2.22	0.67	12.3	-0.346		20481+3718	
20523214+2710274	341	1.84	0.61	28.3	-0.376	-22.2	20503+2658	
20525979+2322159	467	1.08	0.57	71.7	-0.333	9.3	20507+2310	
20534219–0138066	374	3.10	0.62	13.3	-0.306	-17.5	20511–0149	
20545041+4115401	729	3.86	0.84	5.2	-0.341		20529+4104	
20550998+6701580	390	3.88	0.63	12.0	-0.254	-37.6	20545+6650	
20561005+8303252	537	3.01	0.85	26.3	-0.310	32.1	21000+8251	
20575361+4245544	427	3.29	0.82	5.0	-0.556		MSX $^{\ddagger 4}$	
20592292+5853328	730	2.14	0.77	29.3	-0.303	-30.1	20581+5841	
21010281+3932493	386	5.24	0.62	1.9	-0.454		20591+3921	
21010620+5007568	730 †	2.25	0.79	10.4	-0.411		20594+4956	
21013447+5129534	502	4.01	0.81	7.2	-0.327	-35.7	20599+5117	
21045803+2723558	217 ‡	1.72	0.52	31.9	-0.227		21028+2711	
21055966+2924220	270	2.59	0.64	15.4	-0.411	-34.3	21038+2912	
21084764+0110146	730	3.92	0.64	16.4	-0.177	21.8	21062+0058	
21130526+5025299	272 †	2.75	0.71	10.4	-0.303		21114+5013	
21134983+6151234	730 †	2.90	0.69	6.7	-0.406		21126+6138	
21142956+0748337	730	3.94	0.96	34.2	-0.127	28.7	21120+0736	
21174247+4603477	199 †	2.68	0.65	9.6	-0.382		21159+4551	
21182190+4957472	385	3.36	0.81	10.4	-0.363		21166+4945	
21192721+6126125	332	3.73	0.80	7.4	-0.368	-8.0	21182+6113	
21194864+5016575	730	4.63	0.91	9.6	-0.145	-65.0	21181+5004	
21222904+2159543	406	2.47	0.57	16.8	-0.372	2.0	21202+2147	
21231933+2328482	276	2.54	0.60	16.2	-0.309		21210+2316	
21232465+2314598	200 ‡	2.40	0.57	12.4	-0.290		21211+2302	
21254399+4532327	303	4.94	0.78	15.6	-0.276	6.7	21238+4519	

Table 4. (Continued.)

2MASS name (J—)	Period (d)	<i>K</i> mag.	<i>H</i> − <i>K</i>	<i>F</i> ₁₂ (Jy)	<i>C</i> ₁₂	<i>V</i> _{lsr} (<i>SiO</i>) (km s ^{−1})	IRAS/MSX name	comment
21302607+5009190	730	4.75	0.68	6.5	−0.442		21286+4956	
21305815+4629283	294	3.88	0.69	5.4	−0.412	50.0	21291+4616	
21354271+6839071	332	4.91	1.59	10.9	−0.488		21348+6825	
21404842+4949446	337	2.60	0.60	11.7	−0.354	−59.8	21390+4936	
21461997+4806502	443	3.89	0.61	9.4	−0.404		21444+4752	
21485148+3956466	730	3.00	0.69	36.1	−0.163	1.3	21468+3942	
21492590+4322247	419	4.18	0.80	16.8	−0.172	−18.7	21474+4308	
21545410+5128444	327	2.30	0.65	25.6	−0.383	−20.8	21530+5114	
21550333+4945406	630	4.94	0.62	2.2	−0.248	−38.7	21531+4931	
21561897+5848227	162 [†]	3.12	0.71	7.0	−0.271		21547+5834	
21563802+3620341	318	2.86	0.70	11.3	−0.357	−19.3	21544+3606	
21575765+6310007	680	4.68	0.62	5.2	−0.231		21565+6255	
21582612+5324124	730 [†]	4.40	1.11	11.9	−0.408		21566+5309	
22062959+5929281	435 [†]	3.04	0.74	40.5	−0.105		22048+5914	
22063776+5941202	502 [†]	3.68	0.68	15.2	−0.194		22049+5926	
22071622+1153158	584	1.13	0.54	116.5	−0.103	23.3	MSX ^{#5}	
22162185+4744237	492	3.22	0.70	8.0	−0.352	−64.4	22143+4729	
22182648+6705527	169 [†]	4.62	0.89	12.1	−0.268		22170+6650	
22213319+7340270	362 [†]	7.74	0.82	4.2	0.092		22205+7325	
22325976+6654394	164 [†]	2.74	0.73	10.5	−0.321	−9.8	22314+6639	
22361244+7204404	378	3.04	0.82	11.7	−0.168	16.9	22348+7149	
22373599+6116091	285 [†]	3.44	0.64	9.1	−0.194		22357+6100	
22403720+6630334	155 [†]	3.13	0.70	11.9	−0.237		22389+6614	
22470407+5845143	730	4.85	0.95	9.9	−0.149		22450+5829	
22482256+4911596	364	4.60	0.68	6.3	−0.305	−55.2	22462+4856	
22490803+2452563	341	3.29	0.60	9.9	−0.328	−49.7	22467+2437	
22491046+5918129	184 [†]	2.68	0.62	19.0	−0.117		22471+5902	
22502517+6015411	474	3.46	0.64	8.6	−0.288	−62.2	22484+5959	
22504945+6415047	730	1.88	0.71	46.4	−0.318	37.4	22489+6359	
22521809+3413364	235	4.21	0.63	5.8	−0.340	−12.7	22499+3357	
22593446+4250302	256	3.08	0.68	15.6	−0.321	−0.9	22572+4234	
23041981+6745358	592	3.12	0.86	28.5	−0.190	−52.6	23024+6729	
23043019+6445476	317	2.98	0.70	16.5	−0.243	−21.4	23025+6429	
23052739+5707463	437 [†]	2.84	0.62	6.4	−0.367		23033+5651	
23055847+6014593	730 [†]	4.42	0.81	14.6	0.029	−22.1	23038+5958	
23101295+4011462	230 [†]	2.83	0.65	14.0	−0.372	9.3	23078+3955	
23132411−1519163	421	3.08	0.44	8.1	−0.325		MSX ^{#10}	
23143356+5715208	332	3.18	0.72	7.2	−0.376	−15.8	23123+5658	
23162591+3843473	265	3.72	0.61	11.2	−0.196		23140+3827	
23181054+6552436	401	4.35	0.68	3.6	−0.324		23160+6536	
23203705+6732137	106 [†]	3.02	0.77	6.9	−0.289		23185+6715	
23203758+3937140	348	2.01	0.68	33.6	−0.317	−2.0	23182+3920	
23373973+5850458	369	4.10	0.85	10.8	−0.211	−89.9	23352+5834	
23395874+6320547	351	4.17	0.69	1.1	−0.600		23376+6304	
23402236+7026294	155 [†]	2.32	0.65	8.4	−0.462		23380+7009	
23422673+6337387	450	9.04	0.97	1.3	0.390		23400+6320	
23430569+6002467	204 [†]	2.85	0.62	6.0	−0.388		23406+5946	
23430657+3528452	344	3.24	0.67	13.0	−0.225	−25.6	23406+3512	
23520899+6634495	347	2.51	0.61	13.0	−0.370	−59.5	23496+6618	

[†]: semiregular variables (SR+L), [‡]: the other type (MISC); ^{#1} G038.7780−01.1228, ^{#2} G037.3380−02.4122,

^{#3} G082.5317+01.4850, ^{#4} G084.2104−01.8846, ^{#5} G071.9088−34.2583, ^{#6} G084.2104−01.8846,

^{#7} G262.5919+18.5173, ^{#8} G239.6370+55.6395, ^{#9} G182.7804+72.0228, ^{#10} G055.3416-64.3560

^b In IRAS point source reject catalog (Beichman et al. 1989). Reference: ¹ Lewis (1997),

² Crocker & Hagen (1983), ³ Engels et al. (1988), ⁴ Eder et al. (1988), ⁵ Engels & Lewis (1996),

⁶ Lewis (1994), ⁷ Lewis et al. (1990), ⁸ Lewis & Engels (1988), ⁹ Benson & Little-Marenin (1996),

¹⁰ Hall et al. (1990), ¹¹ Parimucha (2003), ¹² Cho & Kim (2010), ¹³ Lewis et al. (1995)

Table 5. Optical and infrared properties of Perseus and Sgr groups of stars.

2MASS name (J—)	Period (d)	type	Rmag (mag)	Amp(R) (mag)	Kmag (mag)	e(K) (mag)	flg(K)	D_L (D_{Lc}) [#] (kpc)	D_K (kpc)
Perseus group									
00163648+6601104	330	M	11.816	2.786	4.241	0.059	E	2.2	5.5
00202547+6947567	425	M	10.993	2.651	2.858	0.246	D	1.2 (1.3)	4.3
00251001+7008516	454	M	11.196	2.933	2.325	0.260	D	1.1 (1.3)	3.6
00365942+6308016	730	M	10.854	2.606	3.073	0.280	D	2.2 (3.9)	5.1
00480999+5334010	298	M	9.469	1.198	2.556	0.362	D	0.9	3.5
01052742+6558594	341	M	10.666	2.690	2.722	0.350	D	1.1	5.8
01070453+4924467	405	M	10.426	2.414	3.184	0.350	D	1.6 (1.6)	5.1
02304255+6635004	467	M	14.287	2.930	5.536	0.020	A	4.4 (5.1)	5.3
02431547+8108095	498	M	10.268	2.584	2.395	0.252	D	1.2 (1.5)	4.8
03323218+7427045	336	M	11.043	2.556	3.716	0.294	D	1.7	4.6
17040522+7147470	336	M	10.483	2.670	3.686	0.036	E	1.7	4.7
20140191+5854355	385	M	12.846	2.293	6.065	9.995 ^b	F	4.9	7.1
21404842+4949446	337	M	9.923	1.997	2.600	0.228	D	1.1	7.0
22162185+4744237	492	M	10.554	2.165	3.218	0.366	D	1.8 (2.2)	7.0
22482256+4911596	364	M	11.262	1.724	4.600	0.018	A	2.7	5.6
22502517+6015411	474	M	11.292	1.052	3.458	0.200	C	2.1 (2.4)	6.0
23041981+6745358	592	M	11.539	3.040	3.123	0.224	D	1.8 (2.6)	4.7
23520899+6634495	347	M	10.538	1.967	2.514	0.304	D	1.1	5.4
Sgr group									
18032344−0218030	594	M	12.061	1.823	4.502	0.015	E	4.1 (5.9)	3.4
18050458+0246114	445	M	10.454	1.988	3.904	0.274	D	2.5 (2.7)	3.5
18223780+0637444	503	M	11.391	1.653	3.328	0.394	D	2.0 (2.5)	4.0
18230711−0146024	476	M	13.330	1.736	4.479	0.348	D	3.3 (3.9)	4.3
18285243+0150161	437	M	12.381	1.678	3.993	0.042	E	2.1 (2.3)	3.5
18335184+0342484	387	M	11.704	1.611	3.288	0.324	D	1.4	2.6
18361528+0126242	354	M	11.820	1.571	3.294	0.228	D	1.1	2.6
18371700+0615306	730	M	12.631	1.712	4.475	0.021	A	4.4 (7.7)	3.1
18373693+1309559	476	M	11.522	2.583	3.060	0.300	D	1.6 (1.9)	4.9
18395233−0423328	730	M	12.468	1.776	3.909	0.036	E	3.6 (6.3)	3.9
18420997+1038548	730	M	11.760	2.022	3.699	0.256	D	3.1 (5.4)	4.7
18422141+0208504	709	M	12.522	2.397	3.154	0.264	D	2.3 (3.9)	3.1
18440224−0638441	349	M	11.000	1.798	3.814	0.236	D	1.9	3.8
18451727+0056300	323	M	12.778	1.570	4.515	0.038	A	2.2	3.9
18482850−0540524	437	M	11.705	1.122	3.707	0.226	D	2.2 (2.4)	3.3
18533423+0048559	221	M	11.567	1.090	3.795	0.260	D	1.3	2.7
19013031+0954055	730	M	12.180	1.250	4.483	0.029	A	4.6 (8.1)	5.9
19030960−0128366	374	M	11.587	1.355	4.611	0.036	E	2.6	3.4
19042996+0305134	587	M	12.856	2.276	4.010	8.888 ^b	F	3.0 (4.3)	2.9
19152147+0233020	331	SR+L	11.564	0.866	4.550	0.024	A	2.5	3.6
19293586+0433277	356	M	12.615	2.914	4.467	0.036	A	2.2	3.2

^b: reliable estimate of the photometric error could not be determined (> 8.0).[#]: parenthetic number is the distance corrected for the HBB stars with $P > 400$ d.